

EFFECT OF APROTIC SOLVENTS ON THE MICROTENSILE BOND STRENGTH OF
COMPOSITE CORE AND FIBER-REINFORCED COMPOSITE POSTS



A Dissertation Submitted in Partial Fulfillment of the Requirements
for the Degree of Doctor of Philosophy in Prosthodontics
Department of Prosthodontics
Faculty Of Dentistry
Chulalongkorn University
Academic Year 2023

ผลของตัวทำละลายอะโปรติก ต่อค่าความแข็งแรงยึดดึงจุลภาคของแกนคอมโพสิตและเดือยฟันคอมโพสิตเสริมเส้นใย



วิทยานิพนธ์นี้เป็นส่วนหนึ่งของการศึกษาตามหลักสูตรปริญญาวิทยาศาสตรดุษฎีบัณฑิต
สาขาวิชาทันตกรรมประดิษฐ์ ภาควิชาทันตกรรมประดิษฐ์
คณะทันตแพทยศาสตร์ จุฬาลงกรณ์มหาวิทยาลัย
ปีการศึกษา 2566

Thesis Title EFFECT OF APROTIC SOLVENTS ON THE MICROTENSILE
BOND STRENGTH OF COMPOSITE CORE AND FIBER-
REINFORCED COMPOSITE POSTS

By Mr. Wisarut Prawatvatchara

Field of Study Prosthodontics

Thesis Advisor Associate Professor NIYOM THAMRONGANANSKUL,
D.D.S., M.SC., PH.D.

Accepted by the FACULTY OF DENTISTRY, Chulalongkorn University in Partial
Fulfillment of the Requirement for the Doctor of Philosophy

..... Dean of the FACULTY OF
DENTISTRY
(Professor PORNCHAI JANSISYANONT, D.D.S., M.S., PH.D.)

DISSERTATION COMMITTEE

..... Chairman
(Associate Professor Awiruth Klaisiri, B.Sc., D.D.S., Ph.D.)

..... Thesis Advisor
(Associate Professor NIYOM THAMRONGANANSKUL, D.D.S.,
M.SC., PH.D.)

..... Examiner
(Assistant Professor PRAROM SALIMEE, D.D.S., Ph.D.)

..... Examiner
(Associate Professor VIRITPON SRIMANEEPPONG, D.D.S.,
M.D.SC., PH.D.)

..... External Examiner
(Assistant Professor Dr. Nantawan Krajangta, B.Sc., D.D.S.,
M.Sc., Ph.D.)

วิศรุตม์ ประวัตินิธิ : ผลของตัวทำละลายอะโปรติก ต่อค่าความแข็งแรงยึดดึงจุลภาค
ของแกนคอมโพสิตและเดือยฟันคอมโพสิตเสริมเส้นใย. (EFFECT OF APROTIC
SOLVENTS ON THE MICROTENSILE BOND STRENGTH OF COMPOSITE
CORE AND FIBER-REINFORCED COMPOSITE POSTS) อ.ที่ปรึกษาหลัก : รศ.ทพ.
ดร.นิยม อารังค่อนันต์สกุล

วัตถุประสงค์ การทดลองนี้มีวัตถุประสงค์เพื่อทดสอบผลของสารละลายอะโปรติก ซึ่ง
ได้แก่ เตตระไฮโดรฟูอราน ไพริดีน และมอร์โฟลีน เมื่อเทียบกับไฮโดรเจนเพอร์ออกไซด์ ต่อความ
หยาบพื้นผิวของ เดือยฟันคอมโพสิตชนิดเส้นใยเสริมแรง และความแข็งแรงยึดดึงจุลภาคระหว่าง
พื้นผิวของเดือยฟันคอมโพสิตชนิดเส้นใยเสริมแรง กับคอมโพสิตก่อกแกน

วิธีการทดลอง เดือยฟันคอมโพสิตเอพาร์ซีโพลีสลาส จำนวน 75 ชิ้น และเดือยฟัน
คอมโพสิตทีไลท์โพส จำนวน 75 ชิ้นถูกแบ่งเป็น 3 กลุ่ม(ไม่ผ่านการเทอร์โมไซคลิง, ผ่านเทอร์โมไซ
คลิง 5,000 รอบ และผ่านเทอร์โมไซคลิง 10,000 รอบ) โดยแต่ละกลุ่มแบ่งเป็น 5 กลุ่มย่อยตาม
การปรับสภาพพื้นผิว ได้แก่ กลุ่มควบคุมที่ไม่มีการเตรียมพื้นผิว, กลุ่มที่เตรียมพื้นผิวด้วยการแช่ใน
ไฮโดรเจนเพอร์ออกไซด์, กลุ่มที่เตรียมพื้นผิวด้วยการแช่ในเตตระไฮโดรฟูอราน, กลุ่มที่เตรียมพื้นผิว
ด้วยการแช่ในไพริดีน และกลุ่มที่เตรียมพื้นผิวด้วยการแช่ในมอร์โฟลีน โดยทุกกลุ่มตัวอย่างผ่านการ
ล้างด้วยน้ำปราศจากไอออน เป่าแห้ง ทาไฮเรนคูกุบ และบอนด์ลง เสียบชิ้นงานตัวอย่างลงในฝา
พลาสติก เติมส่วนคอมโพสิตก่อกแกนจนเต็ม นำชิ้นงานไปตัดแต่ง เพื่อใช้ในการทดสอบความ
แข็งแรงของแรงยึดดึงจุลภาค ภายหลังจากการทดสอบความแข็งแรงพันธะแรงดึงระดับจุลภาคแล้ว
นำชิ้นงานทั้งหมดมาศึกษาแบบของความล้มเหลว ใช้กล้องจุลทรรศน์แบบใช้แสงชนิดสเตอริโอที่
กำลังขยาย 40 เท่า

วิทไธท์ อินเทอร์เพอร์โรมิทรี และ กล้องจุลทรรศน์อิเล็กตรอนชนิดส่อง
กราด ถูกใช้ในการประเมินความหยาบผิวของพื้นผิวของเดือยฟันคอมโพสิตชนิดเส้นใยเสริมแรง นำ
ข้อมูลที่ได้มาวิเคราะห์ทางสถิติโดยใช้การวิเคราะห์ความแปรปรวนทางเดียว และเปรียบเทียบความ
แตกต่างระหว่างกลุ่มด้วยการเปรียบเทียบเชิงซ้อนชนิดทัก และเปรียบเทียบค่าความแข็งแรงพันธะ
สาขาวิชา ทันตกรรมประดิษฐ์ ลายมือชื่อนิสิต
ปีการศึกษา 2566 ลายมือชื่อ อ.ที่ปรึกษาหลัก

6176058832 : MAJOR PROSTHODONTICS

KEYWORD: aprotic solvent, fiber-reinforced composite post, Microtensile bond strength, surface treatment

Wisarut Prawatvatchara : EFFECT OF APROTIC SOLVENTS ON THE MICROTENSILE BOND STRENGTH OF COMPOSITE CORE AND FIBER-REINFORCED COMPOSITE POSTS. Advisor: Assoc. Prof. NIYOM THAMRONGANANSKUL, D.D.S., M.SC., PH.D.

Objective: The purpose of this study was to examine the effect of aprotic solvents, which were tetrahydrofuran, pyridine, and morpholine, compared to hydrogen peroxide on surface roughness of fiber-reinforced composite post and microtensile bond strength between fiber-reinforced composite post surfaces and the composite core.

Material and methods: A total of 75 FRC posts plus, and 75 D.T. light posts were divided into 3 groups (non-thermocycling, 5,000-cycle and 10,000-cycle thermocycling groups). Each group was divided into five subgroups according to the post-surface treatment: C: non-treatment group; H₂O₂: immersing with 35% hydrogen peroxide; THF: immersing with tetrahydrofuran; PY: immersing with pyridine; MP: immersing with morpholine. After 1 minute of immersion, all specimens were rinsed with deionized water, dried with an air blow, silane and bonding agent application, placed in the bottom of the plastic cap, filled with composite core material and prepared specimens for the microtensile bond test. After microtensile testing, Stereo microscope was used to evaluate mode of failure on all specimens at 40x magnification. White light interferometry and scanning electron microscopy (SEM) were utilized to evaluate surface roughness for each surface treatment. A one-way ANOVA was used to analyze all of 3 groups (non-

Field of Study: Prosthodontics

Student's Signature

Academic Year: 2023

Advisor's Signature

ACKNOWLEDGEMENTS

This is to thank the following people: My parents, who always did their jobs and showed me love. To my adviser for “adopting” me as an advisee.

This study was financially supported by a grant from Faculty of Dentistry, Chulalongkorn University, Bangkok, Thailand. The authors gratefully thank Dr. Kevin TOMPKINS for critical review of the manuscript.

Wisarut Prawatvatchara

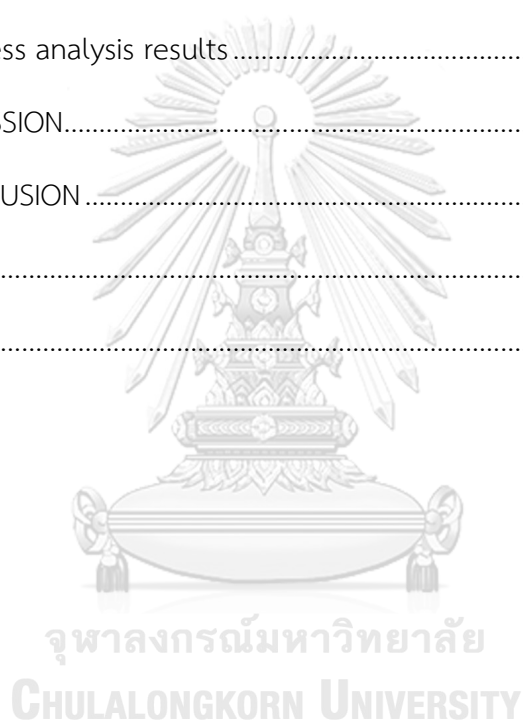


TABLE OF CONTENTS

	Page
.....	iii
ABSTRACT (THAI).....	iii
.....	iv
ABSTRACT (ENGLISH).....	iv
ACKNOWLEDGEMENTS.....	v
TABLE OF CONTENTS.....	vi
LIST OF TABLES.....	ix
LIST OF FIGURES.....	xi
CHAPTER 1 INTRODUCTION.....	1
CHAPTER 2 LITERATURE REVIEW.....	3
2.1 Dental glass fiber-reinforced composite post.....	3
2.2 Dental core-build up materials.....	5
2.3 Surface-treatment chemicals for dental glass fiber post.....	6
2.4 Solubility parameters.....	14
2.5 Interaction between solvent and polymer.....	19
2.6 Multicomponent polymer material.....	20
2.7 Surface roughness.....	23
2.8 Measurement of surface roughness.....	23
2.9 Conceptual framework.....	36
2.10 Research Question.....	36
2.11 Research Objective.....	36

2.12 Research Hypotheses	36
2.13 Proposed Benefits	37
2.14 Related or similar research	37
CHAPTER 3 RESEARCH METHODOLOGY.....	38
Materials and Methods	38
3.1 Materials.....	38
3.2 Equipment	38
3.3 Specimen Preparation.....	39
3.4 Manufacturers and compositions of the materials are presented in Table 11.	43
3.5 Mode of failure evaluation	45
The fracture area was calculated as a percentage of the total bonding area by taking use of the program Image J 1.41 (ImageJ 1.41, Wayne Rasband, National Institutes of Health, Bethesda, Maryland, United States), Cohesive failure was determined to be the mode of failure if the glass fiber post or composite core material interphase was found in more than 60 percent of the total bonding area. They were considered that is mixed failure if the percentage in this region is less than 60 percent but more than 40 percent. In addition, they are considered to have adhesive failure if the above regions composed less than 40 percent of the entire.....	45
3.6 Surface roughness measuring sample preparation.	45
3.7 Sample size calculation.....	47
3.8 Statistical analysis	47
CHAPTER 4 RESULTS	49
The microtensile bond strength	49
No thermocycling condition	49

In terms of the resin matrix type of glass fiber posts, the microtensile bond strength of epoxy resin matrix posts were significantly greater than that of Bis-GMA resin matrix posts across all intervention techniques	49
Thermocycling condition.....	49
The failure modes.....	52
5,000-cycle thermocycling condition.....	52
10,000-cycle thermocycling condition	53
Surface roughness analysis results	56
CHAPTER 5 DISCUSSION.....	59
CHAPTER 6 CONCLUSION	65
REFERENCES	66
VITA.....	84



LIST OF TABLES

	Page
Table 1 shows the chemical and physical data of morpholine.....	10
Table 2 shows the chemical and physical data of Pyridine.....	12
Table 3 The Hansen solubility parameters are as follows.	18
Table 4 shows the Hansen solubility parameters for polymer selection.	19
Table 5 shows the advantages and disadvantages of contact-method surface roughness testing.....	27
Table 6 shows the advantages and disadvantages of AFM (contact mode) for surface roughness measurement.....	28
Table 7 shows the advantages and disadvantages of non-contact methods for surface roughness measurement.....	30
Table 8 displays the benefits and drawbacks of a 3D laser scanning microscope.	31
Table 9 summarizes the properties of white light interferometers.....	34
Table 10 summarizes the differences between contact and non-contact features... 35	
Table 11 exhibits trade names, manufacturers, and compositions of experimental materials.....	43
Table 12 shows the mean microtensile bond strength resulting from non-thermocycling conditions.....	51
Table 13 shows the mean microtensile bond strength resulting after 5,000-cycle thermocycling.....	51
Table 14 displays the mean microtensile bond strength obtained after 10,000-cycle thermocycling.....	52
Table 15 shows failure modes of non-thermocycling condition.	54
Table 16 shows the failure modes of 5,000 thermocycling cycles.	55

Table 17 shows the modes of failure resulting from 10,000-cycle thermocycling. 56

The qualitative evaluations of roughness characteristics using white light interferometry are shown in Tables 18 and 19. In the Epoxy and Bis-GMA groups, treatment with an aprotic solvent (THF, PY, and MP) significantly decreased Ra relative to each control group. Table 18 shows the surface roughness (Ra) of Epoxy groups using white light interferometry. 56

Table 19 displays the surface roughness (Ra) of Bis-GMA groups. using white light interferometry. 57



LIST OF FIGURES

	Page
Figure 1 shows the structure of THF.	7
Figure 2 demonstrates the chemical structure of Morpholine.	9
Figure 3 shows the dehydration of diethanolamine to produce Morpholine.	9
Figure 4 illustrates the Chemical Structure of Pyridine.	12
Figure 5 shows the Hildebrand solubility criterion.	16
Figure 6 exhibits Hansen solubility sphere.	17
Figure 7 shows the six basic combinations of two polymers.	21
Figure 8 depicts the semi-interpenetrating network fabrication approach.	22
Figure 9 shows the process of sequential interpenetrating network syntheses.	22
Figure 10 demonstrates the simultaneous interpenetrating network synthesis.	23
Figure 11 illustrates the graphics of roughness parameter. evaluated included average roughness or Ra parameter, L is the measuring length, M is the mean line. .	24
Figure 12 shows the measuring surface roughness by stylus technique.	25
Figure 13 shows the cone angle and tip radius of stylus.	25
Figure 14 The effect of the grooves which are narrower than the radius of the stylus tip.	26
Figure 15 depicts the discrepancies in measurement outcomes caused by stylus wear.	26
Figure 16 shows the Illustration of an Atomic Force Microscope (AFM) probe tip for surface roughness measurement.	28
Figure 18 demonstrates the plastic cap with a hole in the bottom which a glass fiber post was placed.	40

Figure 19 illustrates a cross-sectional bar-shaped specimen illustration.	40
Figure 20 shows the schematic represent of the specimen attached to the metal grip.	41
Figure 21 demonstrates schematic represent flow chart of specimen preparations.	42
Figure 22 presents a graphic illustration of bond area calculation.	42
Figure 23 shows the schematic representation of all group specimens in the investigation.	43
Figure 27 illustrate the bar graphs depict the failure modes after the 5,000-cycle thermocycling.	55
Figure 28 demonstrates the failure modes are shown by the bar graphs after 10,000-cycle thermocycling.	56
Figure 29 demonstrates the surface topography of Epoxy (D.T. light-post) control and treatment groups, which are hydrogen peroxide, tetrahydrofuran, pyridine, and morpholine, for 1 minute.	58
Figure 30 represents the surface topography of Bis-GMA (FRC post plus) control and treatment groups, which are hydrogen peroxide, tetrahydrofuran, pyridine, and morpholine, for 1 minute.	58

CHAPTER 1

INTRODUCTION

For the purpose of providing core retention, stress distribution, and fracture resistance in endodontically treated teeth with insufficient coronal tooth structure, dental posts are required.

Although the various techniques of fabricating posts and cores can be classified into prefabricated type and custom-cast type, these also divided the materials used for post-fabrication, such as titanium alloy, fiber-reinforced composite, and zirconia. Currently, prefabricated composite posts with fiber reinforcement are frequently employed. Because, when compared to rigid post materials, they have an elasticity modulus that is virtually equivalent to that of dentin. When the tooth, which had a post and core to restore it, came under pressure.

The dentine/composite core interphase was revealed to be a prevalent location for adhesive failure due to the weak bond strength of the two materials. However, the bond strength between the interphase of the post and the composite core is also crucial for securing the core restoration (1, 2, 3). As a result, numerous studies have focused on using chemical or chemo-mechanical treatments to improve the bond strength between dental posts and composite core (4, 5).

From the past to the present, a variety of chemical reagents, including sodium ethoxide, potassium permanganate, hydrofluoric acid and hydrogen peroxide have been investigated for their etching ability to remove polymer matrix. According to the findings of this study, etching with reagent can increase surface roughness and bond strength (1, 6, 7, 8). However, these reagents still have substantial downsides, such as difficult procedures when employing potassium permanganate (9, 10), skin irritation due by high concentrations of hydrofluoric acid and hydrogen peroxide (11, 12), and prolonged immersion time with sodium ethoxide (10, 13). Therefore, the search for a new chemical reagent for glass fiber surface modification was initiated. When predicting the capacity of chemical solutions for etching resin matrix, the solubility parameters are the tools for choosing the best etching solvent agents for

the polymer. In general, solvents can dissolve polymers whose solubility parameters are not drastically different (14). Therefore, the polymer matrix type of fiber post has an influence on the solvent chemical etching; Tetrahydrofuran also takes part in the study (15, 16). While several chemical reagents, such as pyridine and morpholine, have solubility parameters that are extremely close to those of Bis-GMA, which is a part of the polymer matrix in fiber post.

Additionally, neither morpholine nor pyridine were used as etching agents in any dental fiber post research. Therefore, the purpose of this investigation was to evaluate the microtensile bond strength of a composite core and fiber post that had been etched using four different types of chemical agents.



CHAPTER 2

LITERATURE REVIEW

2.1 Dental glass fiber-reinforced composite post

2.1.1 The dental fiber-reinforced composite posts

When compared to other metallic or ceramic posts, the greatest benefit of fiber-reinforced composite posts is their modulus of elasticity (17). Because of the similarity between the elastic moduli of fiber-reinforced composite posts and dentin, will distribute the stress more evenly and are less prone to cause root fracture in teeth that have had endodontic treatment (17, 18, 19, 20).

Fiber-reinforced composite posts can be bonded to the dentinal wall with adhesive or resin cement, which has benefits including lowering the post's tendency to wedge into the root canal and thereby lowering the risk of root fracture (21). Posts built of fiber-reinforced composites are constructed using pre-stretched fibers that are encapsulated in a matrix of resin. Epoxy resin or Bis-GMA matrix are typically used, as well as certain fillers, in fiber-reinforced posts (22, 23).

A Carbon fibers are unidirectional and continuous are impregnated into an epoxy resin matrix but the disadvantage of using carbon-fiber posts is to achieve the ideal aesthetics with all-ceramic restorations (17). Therefore, many manufacturers develop glass-fiber and quartz-fiber reinforced posts for providing aesthetic outcome.

Glass fiber-reinforced composite posts contain quartz-fibers, which are pure silica in crystalline form. Additionally, glass fiber-reinforced composite posts contain E-glass (electrical glass) and S-glass (high-strength glass) (17, 21, 22, 23). According to the manufacturers, these posts have similar biomechanical characteristics to carbon fiber-reinforced composite posts (24, 25, 26); however, some research found that the carbon fiber-reinforced composite posts has better mechanical performances than others (25).

Moreover, they have a hydroxyl group that is capable of silanization (8), This results in improved in the bond strength between the fiber-reinforced composite posts and the composite core interphase (7). The arrangement of the fibers in fiber-

reinforced composite posts gives the posts a high tensile strength, while the resin matrix can withstand compressive stresses (7, 27).

2.1.2 Resin matrix in fiber-reinforced composite posts

The matrix is basically a homogeneous and monolithic material in which a fiber system of a composite is embedded. It bonds the fiber reinforcement, distributes loads among the fibers, and improves the composite's mechanical properties.

A highly cross-linked structure consisting of methacrylate or epoxy polymers makes up the resin matrix of fiber-reinforced composite posts (23).

Epoxy resins are thermosetting polymers that are extensively employed in fiber composites as a matrix material, and they are also used as a resin base for the dental fiber posts (28, 29). However, posts with the epoxy resin matrix had inadequate chemical affinity for the luting resin due to different chemical compositions (10).

The introduction of the aromatic monomer bisphenol A glycidyl methacrylate was the cause for a new revolution in the dental composite posts industry (30).

The use of bisphenol A-glycidyl methacrylate (Bis-GMA) was considered advantageous for enhancing the chemical bonding between the post matrix and that of the resin cement (31). In terms of mechanical properties, the Bis-GMA matrix also has greater flexural strength due to its stiffer nature than that of the epoxy matrix (25, 30).

Surface treatment of fiber posts for increasing bond strength between the fiber-reinforced composite posts and composite core interphase is an interesting topic for several research studies (7, 29, 30, 32). Micro-mechanical and chemical bonding methods were developed using a variety of chemical solutions; however, these approaches lacked selectivity and had the potential to occasionally alter the structure of the post due to the fact that they impacted both the matrix and the fibers (33).

Hydrogen peroxide, sodium ethoxide and potassium permanganate were chosen as chemical reagents because to their potential to partly dissolve resin matrices (34). After the top layer of the epoxy resin has been removed, there will be

a larger surface area of exposed glass fibers that is accessible for silanization. The outcomes of these surface treatments are to be considered favorable (13).

2.2 Dental core-build up materials

Core-build-up materials are the materials placed in the coronal portion of the teeth where natural tooth structure has been lost. In the past ten years, core build-up materials have become increasingly popular, particularly when employing prefabricated posts in teeth that have undergone endodontic treatment.

When used with fiber-reinforced composite posts, the core material is particularly important for the overall success of the restoration of endodontically treated teeth. Several types of materials, such as amalgam, resin composite, glass ionomer cement, and resin modified glass ionomer cement, are the most used core build-up materials.

Nowadays, the most popular core build-up material for fiber-reinforced composite posts is resin composite because it has properties like tooth structure in terms of hardness and fracture toughness (35, 36, 37, 38).

The strength of the composite core materials is influenced by a variety of parameters, including filler particle size, filler loading, amount and type of monomer, intensity and distance of the incident light curing, and irradiation times (38, 39, 40, 41). This may suggest that the strength of the core material alone may not affect the strength of endodontically treated teeth restored with fiber-reinforced composite posts (42). Some studies have shown that several posts and cementation materials have no direct effect on fracture strength or failure patterns. Different circumstances played a role in the study's outcomes, as certain core materials were employed both as cement and as core material (43, 44).

Although debonding of a post restoration at the resin cement/dentin interface is the most common cause of adhesive failure at the restoration's weakest point, only a chemical bond between the fiber post surface and the composite can maintain the connection of the core material around the post at the level of the post-core interface, which influences the stress distribution of the post restoration (8).

The bond strength between the fiber-reinforced composite posts and the core buildup is consequently essential to the success of endodontically treated tooth restorations.

2.3 Surface-treatment chemicals for dental glass fiber post

To achieve better adhesion, a variety of techniques, such as sandblasting and etching with hydrofluoric acid, were used. However, the strength of the posts was reduced because of these approaches, and the structure of the glass fibers was damaged (45, 46, 47).

In order to prevent the integrity of the fiber from being compromised, having identified chemicals that could dissolve only the resin matrix section (8, 10, 12, 48). Potassium permanganate (KMnO_4), sodium ethoxide ($\text{C}_2\text{H}_5\text{ONa}$), and hydrogen peroxide (H_2O_2) were applied in order to etch and disclose the glass fibers (8, 10, 12, 48, 49).

2.3.1 Hydrogen peroxide

Hydrogen peroxide has the chemical formula H_2O_2 . It is considerably more viscous than water, and when pure it is a very light blue color (50). Because of this, it is frequently employed as a diluted solution (3%–6% by weight) in water for consumer use where it functions as an oxidant, bleaching agent, and antiseptic (51), and in greater concentrations where it functions as an antiseptic and bleaching agent (52). Hydrogen peroxide is a reactive oxygen species and the simplest peroxide with an oxygen-oxygen single bond (53). It degrades gradually in the presence of light but degrades rapidly in the presence of organic or reactive chemicals (54).

In immunological electron microscopy, hydrogen peroxide is frequently used to partially dissolve the epoxy resin surface of tissue sections embedded in epoxy resin and expose tissue epitopes for improved immunolabeling (55, 56). For this reason, hydrogen peroxide has been recommended in dentistry for fiber-reinforced composite posts-etching to improve its reactivity to silanization.

Many studies reported that the etching effect of hydrogen peroxide depends on the capacity to partially dissolve the resin matrix, destroying epoxy resin bonds through a mechanism of substrate oxidation (34, 55, 56, 57, 58, 59).

Higher push-out bond strength was obtained after 20 minutes of pre-treatment with 20% H_2O_2 on the post surface before silanization (49).

Monticelli claimed that 10% H_2O_2 for 20 minutes produced a strong connection (29). While another study recommended 24% hydrogen peroxide for 1 min for fiber-reinforced composite posts surface treatment (60). According to research findings, there are numerous procedures; therefore, dentists should select the appropriate and practical fiber-reinforced composite posts-etching technique.

2.3.2 Tetrahydrofuran (THF)

The chemical compound oxolane, also known as tetrahydrofuran (THF), has the formula $(CH_2)_4O$. as shown in Figure 1.

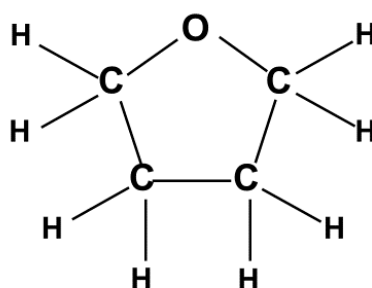


Figure 1 shows the structure of THF.

This substance is categorized as a heterocyclic substance, more specifically as cyclic ether. It is colorless, has a low viscosity, and is water soluble (53, 61). THF is mostly utilized as a polymer precursor. It is a multipurpose solvent since it is polar and has a large liquid range (62). This volatile solvent has a boiling point of 66 °C and a vapor pressure of 176 mm Hg; as a result, high amounts of vapor may occur in the workplace. Compared to other cyclic ethers, its toxicity is believed to be low (53).

Additionally, tetrahydrofuran can be generated via catalytic hydrogenation of furan (63, 64). This enables the conversion of certain sugars to THF through acid-catalyzed digestion to furfural and decarbonylation to furan, however this method is not frequently used (65). THF can therefore be produced using renewable resources.

Applications

It is commonly used as a PVC industrial solvent and in varnishes. Because it has a dielectric constant of 7.6; therefore, it is classified as an aprotic solvent (63). It

is a solvent with a moderate polarity that may dissolve a variety of polar and nonpolar chemical substances (62, 65). THF has also been researched for usage in aqueous solutions as a miscible co-solvent to help liquefy and delignify plant lignocellulosic biomass for the creation of renewable platform chemicals and sugars as potential biofuel precursors (66).

In polymer science, THF is frequently utilized. For instance, polymers can be dissolved with it before their molecular mass is determined using gel permeation chromatography (67, 68, 69, 70).

THF is also the main ingredient in PVC adhesives because it dissolves PVC as well. It is widely used in industry to clean metal parts and can be used to liquefy aged PVC cement (71).

In addition, THF is utilized as a solvent in the 3D printing of Polylactic acid (PLA) plastics (72). It can be used to clean clogged 3D printer components as well as eliminate extruder lines from completed prints and give them a glossy finish.

In the dental field, THF was used as a solvent and surface treatment reagent. We know that THF is an organic, polar, heterocyclic solvent that dissolves a variety of polar and nonpolar substances. These characteristics may support the use of THF in dental adhesives that blend hydrophobic and hydrophilic components. Additionally, THF's volatile nature suggests that it might be easily removed from a surface after application. Fontes et al. (73) showed that THF appears to be a promising solvent for use in dental adhesive systems due to its bond strength stability over time.

Additionally, the combination of THF and silane can increase the shear bond strength of glass fiber posts (15). Consequently, THF is one of the chemical agents that could be used to modify the FRP post surface.

2.3.3 Morpholine

Morpholine is also known as tetrahydro-1,4-oxazine, tetrahydro-2H-1,4-oxazine, diethylene oximide, diethyleneimide oxide, and diethylene imidoxide. Morpholine is a simple heterocyclic 2° amine that has great industrial importance and a variety of uses. It conforms to the formula illustrated in Figure 2 (74).

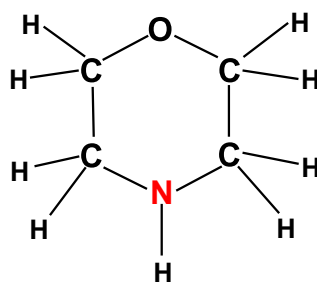


Figure 2 demonstrates the chemical structure of Morpholine.

The dehydration of diethanolamine by a strong acid is one technique for synthesizing morpholine as shown in Figure 3 (75, 76). Concentrated sulfuric acid and concentrated hydrochloric acid are two acids that can be utilized in this procedure. A molar excess of acid is used generally at a temperature over 150°C. An aqueous solution of morpholine is produced by neutralizing the initially acidic reaction mixture with an alkali. By extracting the purified morpholine from the aqueous solution with either an organic solvent or concentrated aqueous alkali, followed by distillation, it can be obtained.

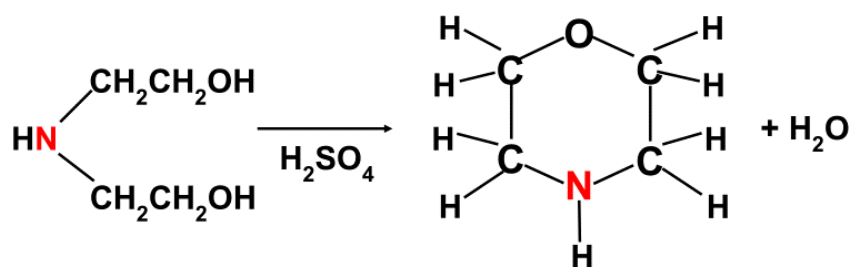


Figure 3 shows the dehydration of diethanolamine to produce Morpholine.

Morpholine is a clear, hygroscopic liquid that can absorb moisture from its surroundings and has a characteristic amine odor (75, 77, 78). It dissolves into several different liquids, including water, methanol, ethanol, benzene, acetone, ether, 2-hexanone, castor oil, ethylene glycol, linseed oil, turpentine, and pine oil. However, concentrated sodium hydroxide solutions cannot dissolve it (78, 79, 80). The chemical and physical data of morpholine are displayed in Table 1.

Table 1 shows the chemical and physical data of morpholine.

Physical form	Colorless, volatile, alkaline, oily liquid
Odor	Amine odor
Formula	C ₄ H ₉ NO
Molecular weight	87.1 2
Assay	99.0% minimum (for cosmetic use) 98% (technical grade)
Vapor pressure	6.6 mmHg at 20°C
Refractive index	1.4537-1.4547 at 20°C
Specific gravity	0.998 at 25°C
Boiling point	1260°C
Viscosity	2.23 centipoises at 20°C
Surface tension	37.5 dynes/cm at 20°C
pH	11.2 (undiluted)
Density	0.999 g/cc at 20°C
Flammability	Flammable

Because of its superior physical, chemical, biological, and metabolic qualities as well as its frequently straightforward synthesis processes, morphine is frequently used in both industrial and medical chemistry (81). In this suggestion, the application of morpholine will be divided into groups for non-cosmetic and cosmetic uses.

Non-cosmetic: Morpholine is used in a broad variety of processes, such as those that produce optical brighteners for detergents, corrosion inhibitors, antioxidants, etc.

Morpholine is also widely employed as a polymerization inhibitor, a step in the process of making rubber, a catalyst for certain chemical reactions, as a corrosion inhibitor in steam condensate systems, as a component of fresh fruit and vegetable protection coverings, as well as a component of waxes and polishes (82).

Cosmetic: Morphine is a common ingredient in cosmetic items like mascara in several countries. In the USA, data submitted to the Food and Drug Administration (FDA) by cosmetic companies participating in the voluntary cosmetic registration program indicated that 38 different cosmetic items that include morphine (83).

Cosmetic product types formulated with this compound included eye shadow, eyeliner, mascara, eye makeup removers and skin care preparations. Mascara is the most common application for morpholine (32 products). Additionally, it is a component in shampoos and other bathroom goods (84).

Studies on human cancer: Data is not available.

Studies of Cancer in Experimental Animals: By administering morphine orally to two strains of mice, one strain each of rats and hamsters, its carcinogenic potential was examined. It was determined that the hamster and one type of mouse studies were insufficient for consideration. No appreciable rise in the prevalence of tumors was observed in treated mice from the other strain. Morpholine was also studied in rats by inhalation exposure, however it had no effect on the frequency of tumors compared to controls (85).

Morpholine is currently found only once in the dental field reported that improved the bond strength of repairing dental resin composites (86). Due to its outstanding properties such as good solvent, high vapor pressure at normal temperatures and high safety. Therefore, its application as a reagent for surface modification of fiber-reinforced composite posts of interest to us.

The chemical formula for pyridine is C_5H_5N . It is a heterocyclic organic molecule with a weak base (87). It has a similar structure to benzene but one of the methine groups ($=CH-$) has been replaced with a nitrogen atom as shown in Figure 4. It is a highly flammable, slightly alkaline, water-miscible liquid with a peculiar, fishy-like odor (88). Pyridine is clear, however older, or impure samples may seem yellow, because long, unsaturated polymeric chains are created, and these chains exhibit significant electrical conductivity (89, 90, 91).

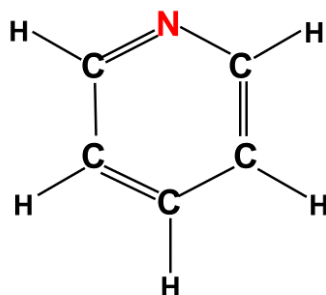


Figure 4 illustrates the Chemical Structure of Pyridine.

The pyridine ring is present in a wide variety of essential substances, such as vitamins, medicines (92), and agricultural chemicals (93). The chemical and physical data of pyridine are shown in Table 2.

Table 2 shows the chemical and physical data of Pyridine.

Physical form	Colorless, volatile, alkaline, oily liquid
Odor	Fish-like odor
Formula	C_5H_5N
Molecular weight	79.1
Assay	99.0% minimum (for cosmetic use) 98% (technical grade)
Vapor pressure	18 mmHg at 20°C
Refractive index	1.5093 at 20°C
Specific gravity	0.998 at 25°C
Boiling point	115.2°C
Viscosity	0.974 centipoises at 20°C
pH	8.81 (undiluted)
Density	0.9819 g/cc at 20°C
Flammability	Flammable

There are numerous uses for pyridine, including as a crucial raw material in the chemical industry, an antibacterial in dental care products, antiviral drugs, etc. (94, 95, 96, 97)

Applications: Pyridine is a polar solvent used for dehalogenation processes as well as the extraction of antibiotics. In addition to being employed as a solvent in the paint and rubber industries (98, 99), pyridine is also used in research labs to extract plant hormones (100).

Dental and Medicine application: Cetylpyridinium and laurylpyridinium, which are utilized as antiseptics in oral and dental care products (101, 102), are made using pyridine as a starting material. A derivative of pyridine monomer, methacryloyloxydodecyl pyridinium bromide (MDPB), is a potent antimicrobial agent present in composites and self-etch adhesives. According to several studies, adhesive systems containing MDPB may protect the hybrid layer by inhibiting MMP (103, 104).

Additionally, the pyridine molecule is a component of many drugs' chemical structures. esomeprazole, which is used to treat gastroesophageal reflux, is one example (105). Another medication made from pyridine known as Claritin, loratadine, is used as a therapy for allergic reactions (106). While Pyridine (phenazopyridine) pills are utilized to treat urinary tract irritation symptoms. Additionally, Phenazopyridine is a dye that acts as an analgesic in the urinary tract (107, 108). In addition, it is utilized to denaturize alcohol and dye various textiles (109, 110).

For the surface treatment of fiber-reinforced composite posts in the pilot study, hydrogen peroxide, morpholine, tetrahydrofuran, and pyridine reagents were utilized. The outcome shown that pyridine can increase the microtensile bond between fiber-reinforced composite posts and core build-up materials.

However, there is still not enough information of some aprotic solvents which are Pyridine and Morpholine for use as surface treatment for enhancing the bond strength between fiber-reinforced composite posts and core build up materials. in addition, the bond strength before and after thermocycling experiments which simulate oral situation. Which is why this research originated. The objective of this research is to explore the effect of aprotic solvent on surface treatments of fiber-reinforced composite posts.

2.4 Solubility parameters

Solubility parameters are numerical values that represent a solvent's relative behavior (111). The energy required to turn a liquid into a gas, known as cohesive energy parameters, is used to calculate solubility parameters. The vaporization energy is a direct measure of the overall energy (cohesive) that holds liquid molecules together (111, 112). In several processing and industrial applications, solubility parameter models are frequently used to choose solvents and non-solvents that are appropriate for polymers.

The Hildebrand and Hansen solubility parameter models, which have both gained widespread acceptance, are the focus of this review. The idea that "like dissolves like" is the foundation of both models (111, 113, 114, 115). This idea helps for polymer science applications such as forecasting the swelling of elastomers by solvents and polymer-binary polymers (binary mixture of polymers) and determining solvent permeation rates (113, 114, 115). There are several factors related to solubility parameters that will be described below.

2.4.1 Solvent and solute molecules attractions

Intermolecular forces are responsible for the cohesion of all material, whether it be liquids or solids. To form a solution, the solvent molecules must overcome the solute's intermolecular force and move between and around the solute molecules (114). At the same time, it is necessary for the solute molecules to effectively separate the solvent molecules from one another. This is most efficiently accomplished when the molecular attractions of both components are equal. If the attractions are distinct enough, strongly attracted molecules will adhere to and exclude less attracted molecules, resulting in immiscibility (114, 115).

2.4.2 Heat of vaporization

The heat of vaporization is the amount of heat necessary to turn one gram of a liquid into vapor without increasing the temperature of the liquid (115, 116).

2.4.3 Van der Waals forces

Van der Waals forces are caused by induced electrical interactions between two or more very near atoms or molecules. These forces, which include dipole-dipole

forces and dispersion forces, are the weakest intermolecular forces.

This polarity characteristic can have an effect on the solubility, which can be explained by the fact that the outer shell of a neutral atom or molecule is exclusively made up of electrons with a negative charge, which surrounds the nucleus, which has a positive charge. Difference in the density of the electron shell will cause a small magnetic imbalance, turning the molecule into a tiny magnet, or dipole. Furthermore, it is created through the interaction of transitory or permanent electric dipole moments.

The degree of polarity is determined by variations in electron density based on the atomic structure of the molecule. Similar polarity substances will dissolve in each other, but when polarity differences increase, solubility becomes increasingly difficult (113, 116, 117, 118).

2.4.5) Cohesive Energy Density

A liquid's cohesive energy density is a measurement of the amount of van der Waals forces holding the liquid's molecules together, represented as vaporization energy in calories per cubic centimeter (118). Because van der Waals forces and vaporization are related, vaporization and solubility behavior are correlated as well (119). The similarity of the intermolecular attractive forces between two substances determines how soluble they are. It seems to reason that substances with comparable cohesive energy density values would be soluble as well. The cohesive energy density can be determined from the heat of vaporization, expressed in calories per cubic centimeter of liquid, using the following formula (115, 120):

$$C = (\Delta H - RT) / V_m$$

C=Cohesive energy density, ΔH =Heat of vaporization,

R=Gas constant, T=Temperature, V_m = Molar volume

2.4.6) The Hildebrand solubility parameter

Hildebrand and Scott were the ones who initially coined the phrase "solubility parameter." To assess whether a material is a good solvent or nonsolvent for a polymer, the Hildebrand model uses a single parameter (δ_t), which is defined as the square root of the cohesive energy density (115, 121). The following equation illustrates the Hildebrand solubility parameter:

$$\delta_t = (E/V)^{1/2}$$

Where E is the pure solvent's (measurable) vaporization energy and V is the solvent's molar volume. The solubility parameter's numerical value in $\text{MPa}^{1/2}$ is 2.0455 times greater than that in $(\text{cal}/\text{cm}^3)^{1/2}$.

The Hildebrand solubility parameter (δ_t) can be a useful tool for determining solubility because it gives a numerical assessment of the level of interaction between two materials, especially for nonpolar substances like many polymers. Materials with comparable values are probably miscible.

The term "nonsolvent" refers to solvents whose δ values deviate from a polymer's by more than $2 \text{ MPa}^{1/2}$. While good solvents are those with values that are within $\pm 2 \text{ MPa}^{1/2}$ of a polymer (122, 123). The Hildebrand solubility criterion is illustrated in Figure 5.

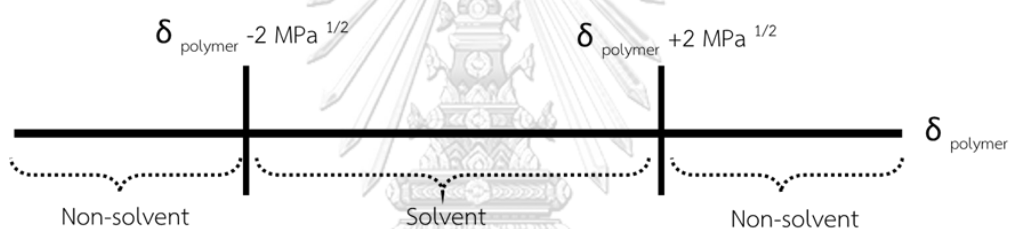


Figure 5 shows the Hildebrand solubility criterion.

However, the fundamental drawback of the Hildebrand parameter is that it disregards specific molecular interactions. (e.g., dipole-dipole interactions). As a result, increasingly complex models, like the three-dimensional Hansen solubility parameters, have been created (121, 122, 123).

2.4.7) Hansen solubility parameter (HSP)

In 1967, Charles M. Hansen developed the Hansen Solubility Parameters (HSP) to predict whether one substance would dissolve in another and form a solution (113, 115, 118, 119).

Hansen suggested extending the solubility parameter in a three-dimensional system. Based on the belief that cohesive energy is the sum of the contributions from molecular interactions with nonpolar, polar, and hydrogen bonds. He partitioned the total solubility parameter into three different components, which are

referred to as the dispersion force component (δ_d), the hydrogen bonding component (δ_h), and the polar component (δ_p) (113, 118, 119, 122). These three parameters (components) can be thought of as coordinates for a point in three dimensions, which is also known as the Hansen space which exhibit in Figure 6. In this three-dimensional space, the closer two molecules are to one another, the more likely it is that they will dissolve into each other.

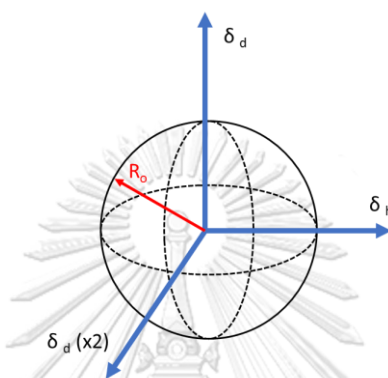


Figure 6 exhibits Hansen solubility sphere.

To ascertain whether a solute lies within the solubility sphere of a given polymer, its distance from the center of the polymer solubility sphere needs to be less than the radius of interaction (R_o) for the given polymer.

Whereas R_o is a distinct property of the necessary solute and can be measured experimentally for each polymer.

Therefore, to calculate the distance (R_a) between Hansen parameters in Hansen space, the following formula is used:

$$\Delta\delta(S-P) \text{ or } R_a = [4(\delta_d^S - \delta_d^P)^2 + (\delta_p^S - \delta_p^P)^2 + (\delta_h^S - \delta_h^P)^2]^{1/2}$$

$\Delta\delta(S-P)$ or R_a = distance between solute and center of solubility sphere

δ^S = Hansen parameter for solvent

δ^P = Hansen parameter for polymer

The system's relative energy difference (RED) is described as follows:

$$RED = R_a / R_o$$

If $RED < 1$, the polymer should be soluble in the solvent.

If $RED = 1$, the polymer should be partially dissolved in the solvent.

If $RED > 1$, the polymer will not be dissolved in the solvent.

HSP was initially created as a useful manual for choosing solvents for coating systems, but it is now utilized in a wide range of industries, including pharmaceutical chemistry (124, 125), molecular biology (126), dental material science (127, 128) and chemical sensing (129, 130, 131).

There are several collections of solubility parameters for solvents and polymers in Table 3. and 4. A select number of solubility parameters data are represented for the solvents and the more important representative classes of polymers utilized in industry and academic investigations (122).

Table 3 The Hansen solubility parameters are as follows.

Solvent	δ_t (MPa) ^{1/2}	δ_d (MPa) ^{1/2}	δ_p (MPa) ^{1/2}	δ_h (MPa) ^{1/2}
n-hexane	14.9	14.9	0.0	0.0
Cyclohexane	16.8	16.8	0.0	0.2
Toluene	18.2	18.0	1.4	2.0
Xylene	18.0	17.8	1.0	3.1
Acetone	20.0	15.5	10.4	7.0
Methyl ethyl ketone	19.0	16.0	9.0	5.1
Methyl isobutyl ketone	17.0	15.3	6.1	4.1
Ethyl acetate	18.1	15.8	5.3	7.2
n-Butyl acetate	17.4	15.8	3.7	6.3
Ethanol	26.5	15.8	8.8	19.4
Pyridine	21.8	19.0	8.8	5.9
Morpholine	21.5	18.8	4.9	9.2
N,N-Dimethylformamide	24.8	17.4	13.7	11.3
Tetrahydrofuran	19.4	16.8	5.7	8.0
Ethylene glycol	32.9	17.0	11.0	26.0

Glycerol	36.1	17.4	12.1	29.3
Dichloromethane	18.5	16.6	8.2	0.4
Carbon tetrachloride	17.8	17.8	0.0	0.6
Water	47.8	15.6	16.0	42.3

Table 4 shows the Hansen solubility parameters for polymer selection.

Polymer	$\delta_t(\text{MPa})^{1/2}$	$\delta_d(\text{MPa})^{1/2}$	$\delta_p(\text{MPa})^{1/2}$	$\delta_h(\text{MPa})^{1/2}$
Epoxy resin	23.75	20.0	10.0	8.0
Bis-GMA	22.1	16.6	13.4	5.8
TEGDMA	19.2	14.2	10.1	8.2
100% HEMA	23.6	13.3	12.3	15.2
Poly(methyl methacrylate)	22.7	18.6	10.5	7.5
Poly(ethyl methacrylate)	18.4	17.6	9.7	4.0

More than solvent selection, HSP was used in applications for explaining problems that are involved in mixing or diffusion phenomena, including swelling behavior and the prediction of environmental stress cracking in plastics (132) and the optimization of polymer additives.

2.5 Interaction between solvent and polymer

A solvent contact with a polymer, the solvent diffuses into the polymer, causing the polymer surface to swell (133, 134). The rate of diffusion is influenced by a number of factors, including time, temperature, the nature of the solvent, the structure of the polymer, and the glass transition temperature (T_g) of the polymer (135).

The process of solvent diffusion into a polymer might take place in one of two distinct ways depending on the type of polymer. When a polymer is amorphous

and its temperature is above the glass transition temperature, the diffusion of the solvent into the polymer forms a smooth composition curve, with the most highly swollen material located at the outside border.

In this circumstance, diffusion within the glassy polymer is slow. The solvent must first plasticize the polymer by reducing its glass transition temperature to below ambient. Then, rapid swelling ensues. Extremely swollen material and considerably non-swollen material are separated by a boundary that is quite distinct and constantly shifting. Typically, the tension near the swelling border is responsible for the sample cracking or breaking. This similar effect is observed with semicrystalline polymers.

If the polymer is cross-linked, it will only swell until it reaches a state of equilibrium (134, 135).

2.5.1) Swelling Phenomena

The definition of swelling is the penetration of a solvent into a polymer network, which results in an abrupt change in volume (136). When a polymer has contact with a solvent. There is polymer to solvent diffusion and solvent to polymer diffusion. As a minute solvent molecule, the diffusion rate of the solvent is considerably increased. The degree of crystallinity, cross-linking, and the strength of attracting and repulsive forces can influence the intensity of the swelling (134, 137, 138).

Consequently, the polymer interacts with the solvent for a period. If the polymer is glassy, the solvent reduces the T_g through a plasticizing effect. polymer molecular motion increases (139).

2.6 Multicomponent polymer material

When two or more polymers are combined, a basic six-polymer combination is formed, as shown in Figure 7. (140, 141).

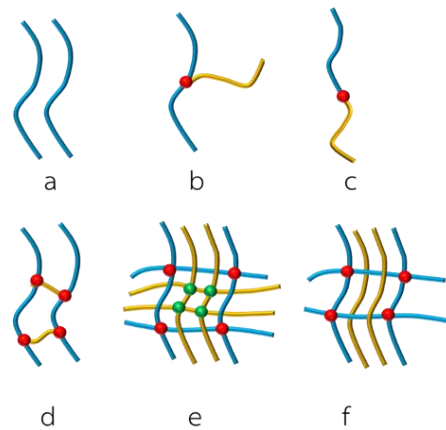


Figure 7 shows the six basic combinations of two polymers.

a, Polymer blend, no bonding between chains; b, a graft copolymer; c, a block copolymer; d, and graft copolymer; e, an IPN; f a Semi-IPN.

2.6.1) Interpenetrating Polymer Network (IPN)

An interpenetrating polymer network (IPN) is a type of polymeric system in which there are no covalent interactions between two or more polymeric networks that are at least partially interlocked at the molecular level (139, 140).

Semi- interpenetrating networks (semi-IPN) Compositions that contain one or more cross-linked polymers and one or more linear or branched polymers. In dentistry, acrylic resin is introduced as restorative materials. These materials are prepared from two components to form a semi-IPN polymer that is made up of linear poly (methyl methacrylate) as polymer B and MMA monomer plus crosslinking agents as network A (133, 141, 142). The technique begins with the synthesis of a crosslinked polymer A. The monomer B and initiator are then swelled into polymer A and polymerized in situ, as shown in Figure 8.

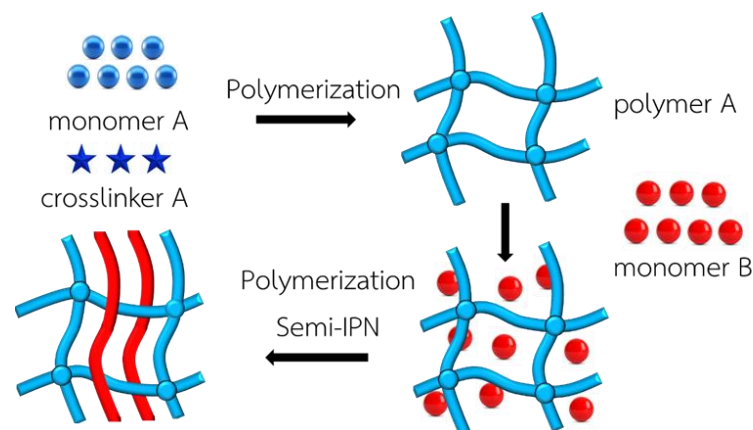


Figure 8 depicts the semi-interpenetrating network fabrication approach.

However, interpenetrating polymer network creation can be classified into sequential and simultaneous interpenetrating networks.

2.6.2) The sequential interpenetrating networks

The procedure starts with the creation of a crosslinked polymer A. After that, the monomer B, plus its own crosslinker and initiator, are swollen into polymer A and then polymerized in situ, as shown in Figure 9.

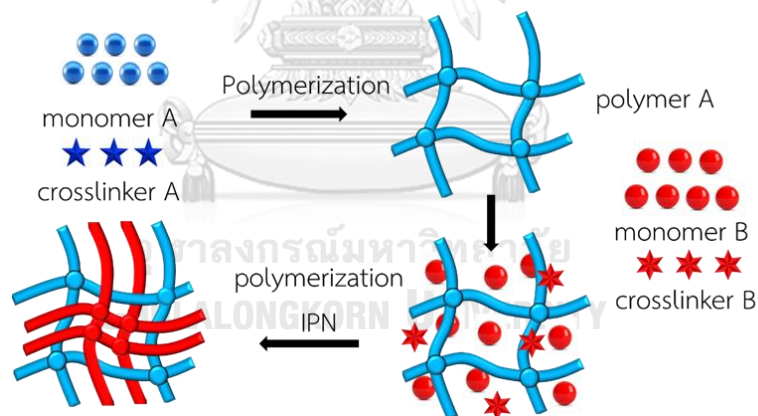


Figure 9 shows the process of sequential interpenetrating network syntheses.

2.6.3) The simultaneous interpenetrating networks

Differ from above, beginning with a solution of monomers and crosslinkers that are polymerized simultaneously by noninterfering modes as Figure 10.

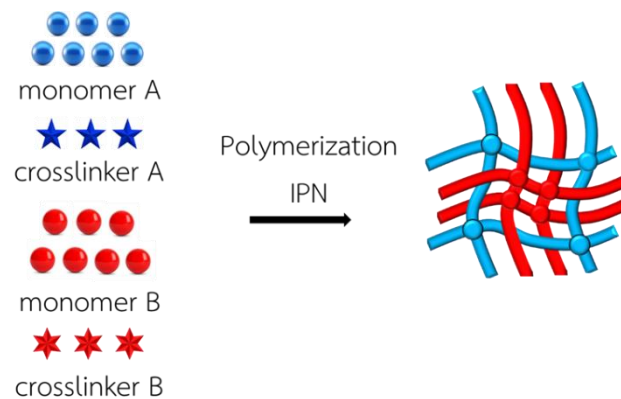


Figure 10 demonstrates the simultaneous interpenetrating network synthesis.

2.7 Surface roughness

Surface roughness, often known as surface texture, is defined as the irregularities that occur throughout the manufacturing process. It could be caused by vibrations, work deflections, and strains in the material. Roughness is often regarded as the high-frequency, short-wavelength part of a measured surface in surface metrology (143).

In tribology, rough surfaces often wear faster and have greater friction coefficients than smooth ones. Roughness is frequently a useful predictor of mechanical component performance because surface irregularities might act as nucleation sites for fractures or corrosion. Roughness, on the other hand, may encourage adherence (144).

2.8 Measurement of surface roughness

Arithmetic average roughness or Ra parameter refers to the arithmetic mean of the absolute values of vertical deviation from the mean line through the profile within the measuring length, as shown in Figure 11 (143). In the dentistry sciences, the Ra or arithmetic average roughness parameter is commonly utilized as an evaluation metric.

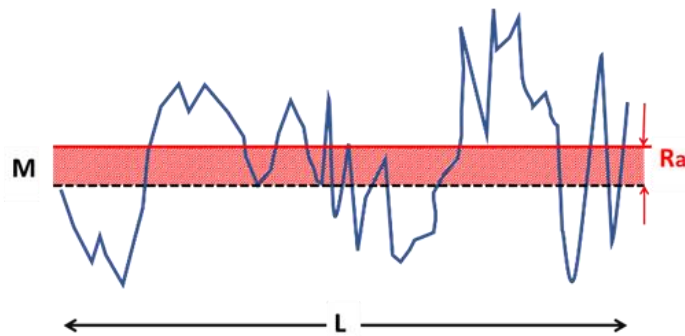


Figure 11 illustrates the graphics of roughness parameter. evaluated included average roughness or Ra parameter, L is the measuring length, M is the mean line.

For the surface treatment methods which applied to dental material significantly affect the bond strength. Increasing bond strength may correlate with a rise in average surface roughness (144). Profilometry is usually used to assess the surface roughness of dental materials.

Profilometry: A profilometer is a measuring topographical technique which used to analyze a surface's profile, to get surface morphology, step heights and surface roughness (143). A single point, a line, or even a complete three-dimensional scan can be used for this. Profilometry can be derived into two types of methods, which are contact and non-contact profilometry.

2.8.1 Contact profilometry.

Instruments for measuring surface roughness using the contact technique are made up of the tip of a stylus that comes into direct contact with a specimen's surface. The stylus is parallel to the sample's surface during tracing a surface, and electrical sensors pick up the stylus' vertical movement. as shown in Figure 12 (145, 146). The electrical signals are amplified and digitally converted before being recorded.

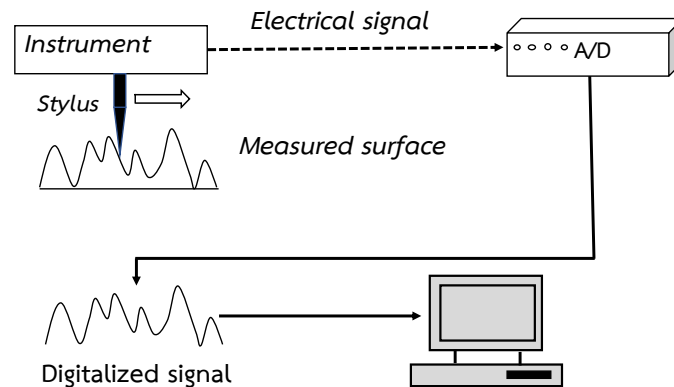


Figure 12 shows the measuring surface roughness by stylus technique.

Using a contact-method surface roughness tester to properly measure delicate forms and roughness, The radius of the stylus tip must be as tiny as feasible while maintaining low contact pressure. Styluses are commonly made of sapphire or diamond, with a tip radius of 1.5–2.5 μm (146). A stylus with a conical shape and a ballpoint tip is thought to be suitable. As demonstrated in Figure 13, the smallest profiles that a stylus is able to trace are determined by the cone angle as well as the tip radius. These measurements which are based on the use of a sharp tip are influenced by the size and form of the stylus tip (144, 145, 146, 147, 148, 149).

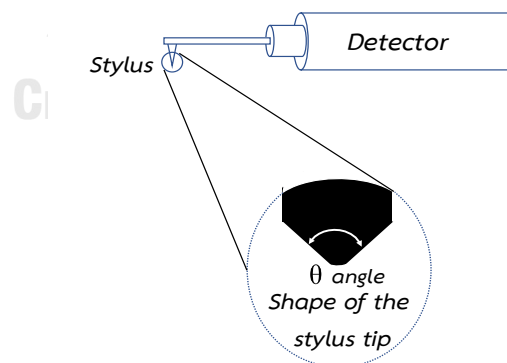


Figure 13 shows the cone angle and tip radius of stylus.

This technique has limitations, for example taking more analysis time than non-contact techniques, The spherical stylus tip cannot trace the groove, which is narrower than the radius of the stylus tip, as shown in Figure 14.

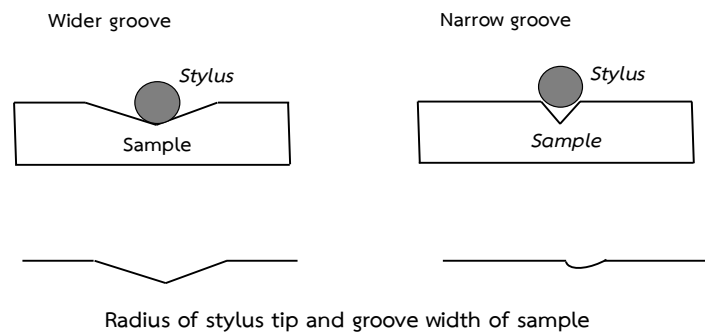


Figure 14 The effect of the grooves which are narrower than the radius of the stylus tip.

In general, the stylus tips made of wear-resistant materials such as diamond or sapphire can damage and may leave micro-scratches on testing surfaces (150), however, as time passes, the stylus's tip wears down and must be polished. The pattern of wear varies, thus depending on the material and form of the target object for measurement, the stylus tip might become flat or rounded. Different stylus shapes result in fundamentally distinct wave characteristics. A commercially available wear-inspection test piece can be used to determine stylus wear. Figure 15 depicts a comparison of the data profile (groove width) of the test piece before and after stylus wear.

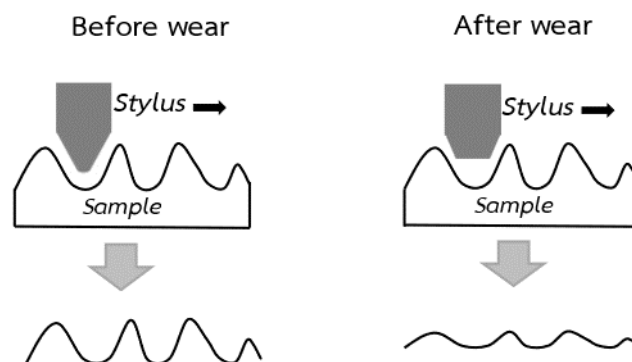


Figure 15 depicts the discrepancies in measurement outcomes caused by stylus wear.

Moreover, the stylus cannot maintain contact and precisely align the profilometer trace along a cylindrical surface (144, 151, 152).

As illustrated in Table 5, direct contact with a sample typically entails several disadvantages.

Table 5 shows the advantages and disadvantages of contact-method surface roughness testing.

Advantages	Disadvantages	
- A distinct wave profile	- the deterioration of the stylus tip	
- Long-distance measurement capability	- Pressure measurement might result in scratches on the sample surface	
	- The radius of the stylus tip limits the measurement.	
	- Impossibility of quantifying viscous samples	
	- Difficulties in identifying and locating delicate measuring points	
	- It takes time	
	- Sample cutting and processing are required for detector tracing.	

Atomic force microscopes (AFM) in contact mode

Using the atomic forces between the tip and the sample, the atomic force microscope (AFM) calculates the roughness of a sample. The user positions the cantilever, which has a probe at one end and a sharp tip at the other, in close contact to a sample surface to take measurements. Throughout scanning, a constant force is maintained between the tip and the sample. A laser beam is emitted from the rear side of the cantilever, and the reflected beam is detected by two- or four-segment photodiodes as shown in Figure 16. This optical lever method generally is

used to measure the deflected cantilever during giving the piezo scanner feedback. The z-axial displacement, which represents the surface structure, is determined by measuring the feedback displacement from the piezo scanner.

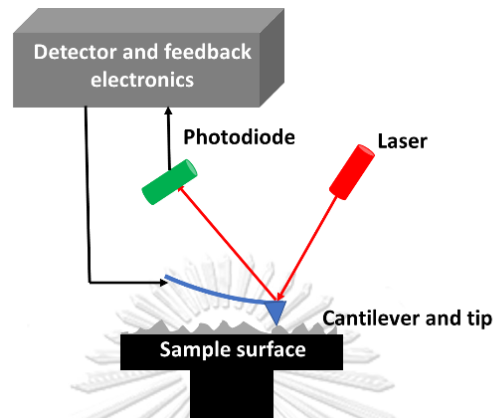


Figure 16 shows the Illustration of an Atomic Force Microscope (AFM) probe tip for surface roughness measurement.

An AFM creates images by scanning a tiny cantilever across a sample's surface. The cantilever's pointed tip makes contact with the surface, bending it and adjusting the intensity of laser light reflected into the photodetection. The cantilever height is then modified to reestablish the response signal, with the measured cantilever height tracking the surface.

AFM has been used to assess erosion in human enamel, and this has been shown to be an appropriate instrument for assessing the early phases of enamel demineralization (153).

The advantages and disadvantages of AFM (contact mode) are outlined in Table 6.

Table 6 shows the advantages and disadvantages of AFM (contact mode) for surface roughness measurement.

Advantages	Disadvantages

It provides high resolution on the nanoscale.	The vertical range is limited.
Sample preparation is kept to a minimum.	Images that have been distorted as a result of lateral forces.
When compared to other operation modes, the scan speed is fast.	Soft sample distortion as a result of strong probe-surface interactions.

It is becoming more and more important to produce the most precise control approaches as requirements for improving the quality of metrological methods rise. The improvement of the frequently used stylus instruments has attained a high level of technicality. One of the main drawbacks of these mechanical profilometers is that a tip must make mechanical contact with the surface being measured, yet this requirement raises the possibility of soft material damage. Unwanted resonance frequencies of the measurement tip as it passes over the surface restrict their accuracy and sensitivity. By adopting non-contact measurement methods that can be created based on optical principles, these drawbacks can be virtually avoided. Several non-contact optical and non-optical methods have been developed.

2.8.2 Non-contact profilometry

Non-contact profilometry involves the use of light or sound. Optical devices such as white light and confocal replace the stylus. These devices employ various measurement principles. Some non-contact equipment is made from repurposed contact-type detectors by replacing the physical probe with microscopes and optical sensors (154).

This device will initially transmit an ultrasonic pulse to the surface. After then, the sound waves will be changed and reflected to the device. The roughness parameters can then be calculated using the reflected waves. Non-contact methods

include structured light, electrical capacitance, electron microscopy, interferometry, confocal microscopy, focus variation, atomic force microscopy (non-contact method), and photogrammetry (155).

Furthermore, light can be used to assess surface roughness by shining a laser beam onto the surface and measuring the intensity of the reflected light. The rougher the surface, the lighter is scattered, and the less light is reflected. The following Table 7 summarizes the characteristics of non-contact approaches.

Table 7 shows the advantages and disadvantages of non-contact methods for surface roughness measurement.

Advantages	Disadvantages
-There is no surface damage to the sample.	Target measurement size is limited. (Some microscope types)
- Non-contact method has less asperity than contact method	
- Rapid measurements	
- Surface image and height profile observation at the same time (microscope type)	
- Capable of acquiring high-definition, fully focused images comparable to those obtained by SEM (color 3D laser microscope)	

Optical profilometry

The optical profilometer is a type of microscope that uses a light source to analyze the surface's topography. A beam splitter is placed between the objective and the sample of an optical microscope to divide light into two paths. One path directs light to the sample's surface, while the other directs light to a reference mirror just below the objective lens. Reflections from the sample surface and the

mirror are recombined to generate interference fringes, which are projected onto an array detector (151).

Having a surface that can reflect the light beam is crucial for this technique to work, which means that it is often necessary to modify the sample surface in order to get a more accurate reflection.

There are numerous data collection methods, including focus variation, white light interferometry, and laser scanning confocal microscopy (152).

Laser microscopes for measuring surface roughness.

A 3D laser scanning microscope is a type of observation/measuring device that can perform 3D measurements as well as deep focus depth observations at the same time. It allows for observations under typical environmental conditions and has no limitations on sample size or composition. A user-friendly interface like that of an optical microscope is also present in the 3D laser scanning microscope (155, 156); materials do not need to be pretreated before measurement. Color observations can be made, which aids in the correct analysis of the target object's conditions. A 3D laser scanning microscope can also be used to check the surface, inside, and opposite of a translucent item, as well as to measure the thickness of films. (157).

While the 3D laser scanning microscope outperforms a SEM or an AFM in terms of operability, it falls behind in terms of observation magnification and measurement resolution. Bottom areas with high aspect ratios and steep slopes cannot be measured or identified because they do not reflect the laser beam. Table 8 summarizes the features of a 3D laser scanning microscope.

Table 8 displays the benefits and drawbacks of a 3D laser scanning microscope.

Advantages	Disadvantages
- The deep focus	- Capable of high-definition observation and accuracy measurements down to 1 nanometer.
- Color images of the target object are available.	- Data cannot be gathered from sample surfaces (such as the sides) that do not receive laser beam emission.

- Creates 3D profiles and displays color 3D images	- Materials that absorb laser beam wavelength cannot be measured.
- Capable of determining the thickness of a translucent object's film	
- Analysis under atmospheric conditions is possible, with no sample pretreatment required.	
- There are no restrictions on sample size or material, and the simple operation makes it ideal for general-purpose use.	

White Light Interferometry (WLi)

White light interferometry is an optical profilometry technique that is selected over monochromatic light due to its shorter coherence length, which provides higher accuracy (152, 158, 159).

Light interference happens when the light travels a different distance from the surface of a target item to a specific spot. Figure 17 depicts the fundamental architecture of white light scanning interferometry

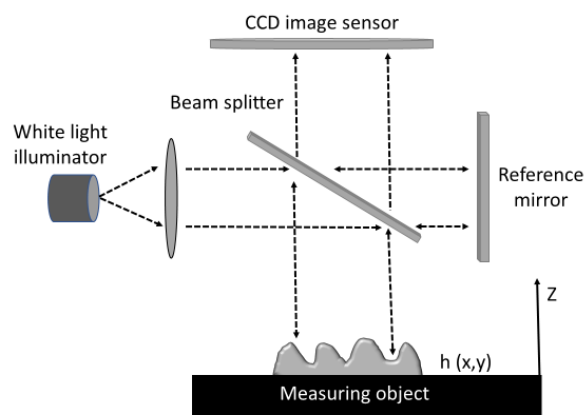


Figure 17 illustrates the fundamental arrangement of white light scanning interferometry.

The white light emitted by the source is divided into beams: measurement beam and reference beam. The measurement beam is reflected to the sample surface, whilst the reference beam travels through the reference mirror via a beam splitter. The reference mirror reflects the passing beam onto the CCD image sensor, creating an interference pattern. The other beam is reflected off the surface of the sample, goes through the beam splitter, and generates an image using the CCD image sensor. Through the CCD image sensor (160, 161, 162).

White Light Interferometry is easier, faster, and more accurate than other optical methods. It can also cover a larger image area than atomic force microscopy (151, 163).

White light interferometry was used to analyze erosion enamel (164), etched enamel (165) and surface characteristics of implant materials (166, 167). However, these were not reported regarding glass fiber following analysis of surface roughness with white light interferometry. The characteristics of white light interferometers can be summarized as shown in table 9.

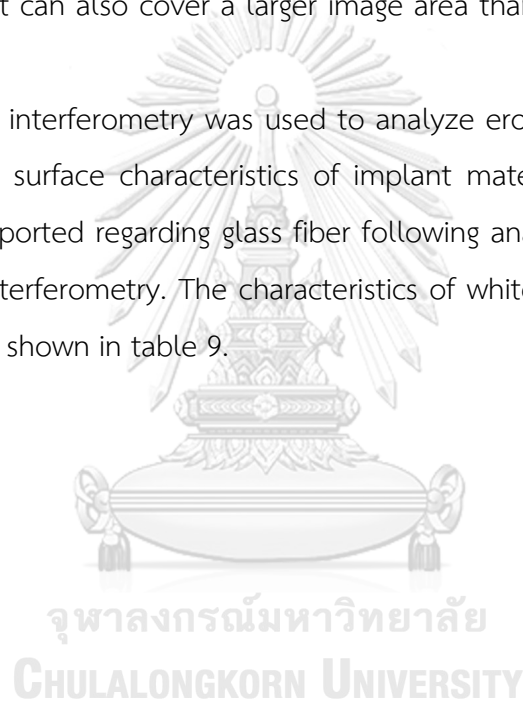


Table 9 summarizes the properties of white light interferometers.

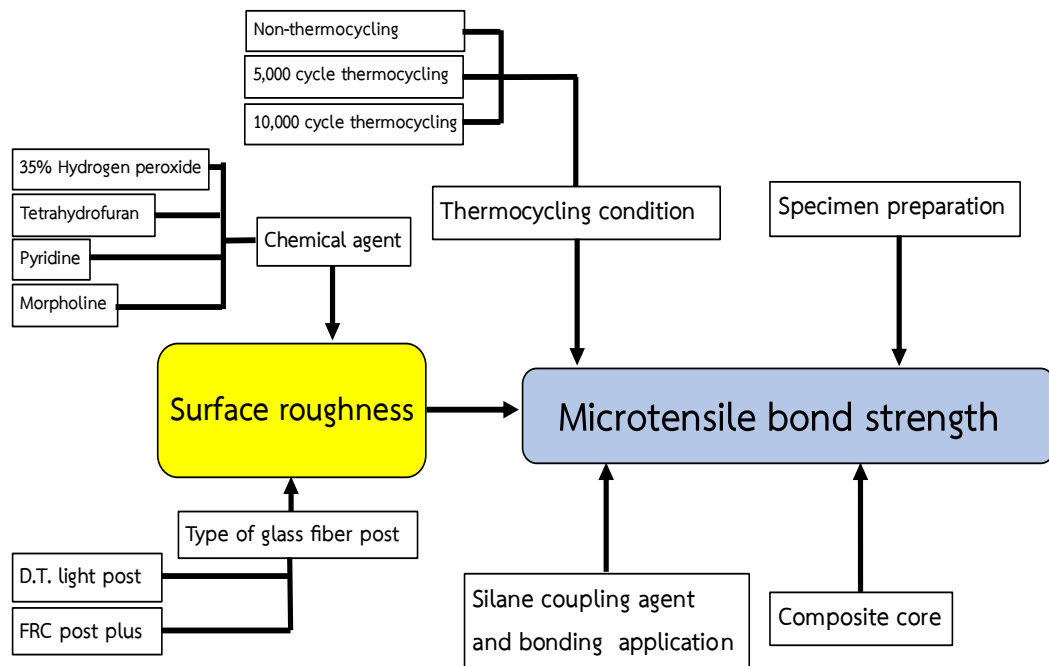
Advantages	Disadvantages
<p>- Capable of measuring a large field of vision</p> <p>It is feasible to measure in the sub-nanometer range.</p>	<p>- There is only a limited angular feature.</p>
<p>- Quick measurement</p>	<p>- The application is limited to particular items. White light interferometers are only able to detect when there is a strong reflection. There, measuring capabilities on a diverse assortment of things are not supported.</p> <p>Measurements may also be impossible if the light reflected from the reference mirror differs significantly from the light reflected from the measurement area.</p>
	<p>- Adjustment of the tilt is necessary. Before measurement, a goniometric stage must be employed to correct sample tilt. Tilted samples may result in closely spaced interference patterns, hence decreasing the precision of measurements. Some white light interferometry systems have a tilt mechanism that automatically corrects sample tilt.</p>
	<p>- Sensivity to vibrations Due to the equipment's extreme vibrational sensitivity, installation choices are restricted. Installation calls for shock-absorbing tables.</p>

There is numerous measurement equipment on the market for analyzing and evaluating surface roughness. The characteristics of contact and non-contact can be summarized as shown in table 10.

Table 10 summarizes the differences between contact and non-contact features.

Method	Contact		Non-contact	
Instrument for measuring	Roughness tester of contact type	Atomic force microscope (AFM)	White light interferometer (WLi)	Laser microscope
Resolution of measurement	1 nanometer	< 0.01 nanometer	< 0.1 nanometer	0.1 nanometer
Height measurement range	1 millimeter or less	< 10 micrometer	< a few millimeter	< 7 millimeter
Range that can be measured	a few of millimeters	1 to 200 micrometer	40 micrometer to 15 millimeter	15 micrometer to 2.7 millimeter
An angular feature	-	Poor	Fair	Good
An angular characteristic	-	VGA	VGA	SXGA
Samples are damaged.	Contact	Contact	Non-contact	Non-contact

2.9 Conceptual framework



2.10 Research Question

Would the different etching agents have an effect on microtensile bond strength of composite core and different fiber posts type?

2.11 Research Objective

To assess the microtensile bonding strength between two distinct types of fiber posts and a composite core using various etching chemicals.

2.12 Research Hypotheses

H₁₀: There is no difference of microtensile bond strength between composite core and fiber post using different etching agents.

H₁₁: There is difference of microtensile bond strength between composite core and fiber post using different etching agents.

H₂₀: There is no difference of microtensile bond strength between composite core and different type of fiber post using different etching agents.

H₂₁: There is difference of microtensile bond strength between composite core and different type of fiber post using different etching agents.

H3₀: There is no difference of microtensile bond strength between composite core and each type of fiber post using different etching agents before and after 5,000 and 10,000-cycle thermocycling.

H3₁: There is difference of microtensile bond strength between composite core and each type of fiber post using different etching agents before and after 5,000 and 10,000-cycle thermocycling groups.

H4₀: There is no difference in surface roughness of each type of fiber post using different etching agents.

H4₁: There is no difference in surface roughness of each type of fiber post using different etching agents.

2.13 Proposed Benefits

To suggest etching agents that provide the maximum microtensile bonds strength between two different types of fiber posts and a composite core.

2.14 Related or similar research

There has not been any study on the surface modification of fiber-reinforced composite posts with Tetrahydrofuran, Pyridine and Morpholine.

CHAPTER 3

RESEARCH METHODOLOGY

Materials and Methods

3.1 Materials

1. FRC post plus; Ivoclar Vivadent, Schaan, Liechtenstein
2. D.T. light- post; Recherches Techniques Dentaires, RTD, St. Egreve, France
3. Multicore Flow; Ivoclar Vivadent, Schaan, Liechtenstein
4. Excite DSC; Ivoclar Vivadent, Schaan, Liechtenstein
5. Monobond plus; Ivoclar Vivadent, Schaan, Liechtenstein
6. Tetrahydrofuran; LOBA Chemie Pvt. Ltd. - Jehangir Villa, 107, Wode House Road, Colaba, Mumbai, India
7. 35% Hydrogen peroxide;
8. Pyridine; LOBA Chemie Pvt. Ltd. - Jehangir Villa, 107, Wode House Road, Colaba, Mumbai, India
9. Morpholine; LOBA Chemie Pvt. Ltd. - Jehangir Villa, 107, Wode House Road, Colaba, Mumbai, India
10. Model repair ll; Sankin industry, Tokyo, Japan
11. deionized water
12. forcep
13. glass slide
14. plastic cup
15. microbrush

3.2 Equipment

1. Universal Testing Machine; EZ-S 500N, Shimadzu Corporation, Kyoto, Japan.
2. Light curing unit; Bluephase N[®], Ivoclar Vivadent, Schaan, Liechtenstein.
3. Ultrasonic cleaner; Branson5210, Branson, CT, USA.
4. Stereo Microscope; SZ61, Olympus Corporation, Tokyo, Japan.
5. Gold sputtering unit; JFC-1200E Fine coater, JEOL Ltd., Japan.

6. Scanning Electron Microscope; Quanta 250, FEI Company, Oregon, U.S.A.
7. Slow speed cutting machine, Model Isomet, Buehler, IL, U.S.A.
8. Digital Vernier caliper ;Mitutoyo series 500, Japan
9. The metal grip for Universal Testing Machine to microtensile test
10. The White Light optical interferometry; WLI, ContourX-1000, Bruker, Salbruken, Germany.

3.3 Specimen Preparation

150 fiber-reinforced composite posts with a maximum diameter (size 3) consisting of 75 FRC plus posts and 75 D.T. light-posts. Each set of fiber-reinforced composite posts was separated into 3 subgroups (non-thermocycling 5,000-cycle and 10,000-cycle thermocycling group). Before testing, all specimens were immersed in 24°C water with ultrasonic cleaner (Branson5210, Branson, CT, USA.) for 5 minutes and stored in a dry place.

According to the post surface treatment, the non-thermocycling group was subdivided into the following five subgroups:

Subgroup 1:

C: non-etching group, rinsed with deionized water, dried with air blow, silane application

Subgroup 2:

H₂O₂: immersed in 35% hydrogen peroxide for 1 minute, rinsed with deionized water, dried with air blow, silane application.

Subgroup 3:

THF: immersed in tetrahydrofuran for 1 minute, rinsed with deionized water, dried with air blow, silane application.

Subgroup 4:

PY: immersed in pyridine for 1 minute, rinsed with deionized water, dried with air blow, silane application.

Subgroup 5:

MP: immersed in Morpholine for 1 minute, rinsed with deionized water, dried with air blow, silane application.

Then, an identical technique for all subgroups was used: All specimens were placed into the hole in bottom of plastic cap as display in Figure 18. Excite F DSC (Ivoclar Vivadent, Schaan, Liechtenstein) was applied for 10 seconds with a microbrush for only thin layer and the excess bonding agent was removed with gently air-dried, then polymerization with light curing unit (Bluephase N[®], Ivoclar Vivadent, Schaan, Liechtenstein), with high intensity, for 20 seconds.



Figure 17 demonstrates the plastic cap with a hole in the bottom which a glass fiber post was placed.

Multicore flow (Ivoclar Vivadent, Schaan, Liechtenstein) was injected around the post until fully fill in plastic cap and light cured for 40 seconds per surface. All specimens were stored in dry environment for 24 hours at 37 °C before section into 1 x 1 mm² cross-sectional bar shape by a slow-speed diamond machine (Model Isomet, Buehler, IL, USA) and were measured with Digital Vernier caliper (Mitutoyo series 500, Japan) as shown in Figure 19.

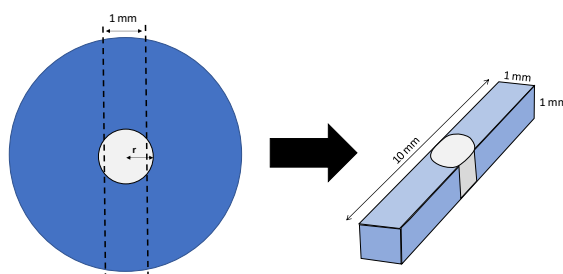


Figure 18 illustrates a cross-sectional bar-shaped specimen illustration.

Thermocycling group was divided by different treatment agents into 5 subgroups (Ctmc, H₂O₂tmc, THFtmc, PYtmc and MPtmc) as same Non thermocycling group.

The thermocycle specimens were 10,000-cycle thermocycling between water baths at 5 degrees °C and 55 degrees °C, with a dwell time of 60 seconds in each.

Each of specimen was attached to the metal grip as shown in Figure 20, which can assemble with Universal Testing Machine (EZ-S 500N, Shimadzu Corporation, Kyoto, Japan) with cyanoacrylate glue (Model repair II; Sankin industry, Tokyo, Japan) and tensile strength loaded at a crosshead speed of 1 mm/min until failure occurred.

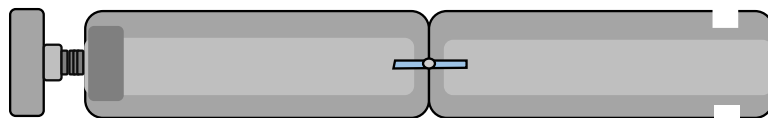


Figure 19 shows the schematic represent of the specimen attached to the metal grip.

Each step of the specimen preparation procedure is illustrated in Figure 21.

The microtensile bond strength was determined by the applied tension divided by the bonded area. But the post-composite core interface is curved, this area was measured by using the mathematical formula described; $A = 2r \arcsin(L/2r) \times h$, where r , L , and h are the diameter, width, and thickness of the post, shown in Figure 22. While Figure 23 was a schematic depiction of all group specimens collected during the investigation.

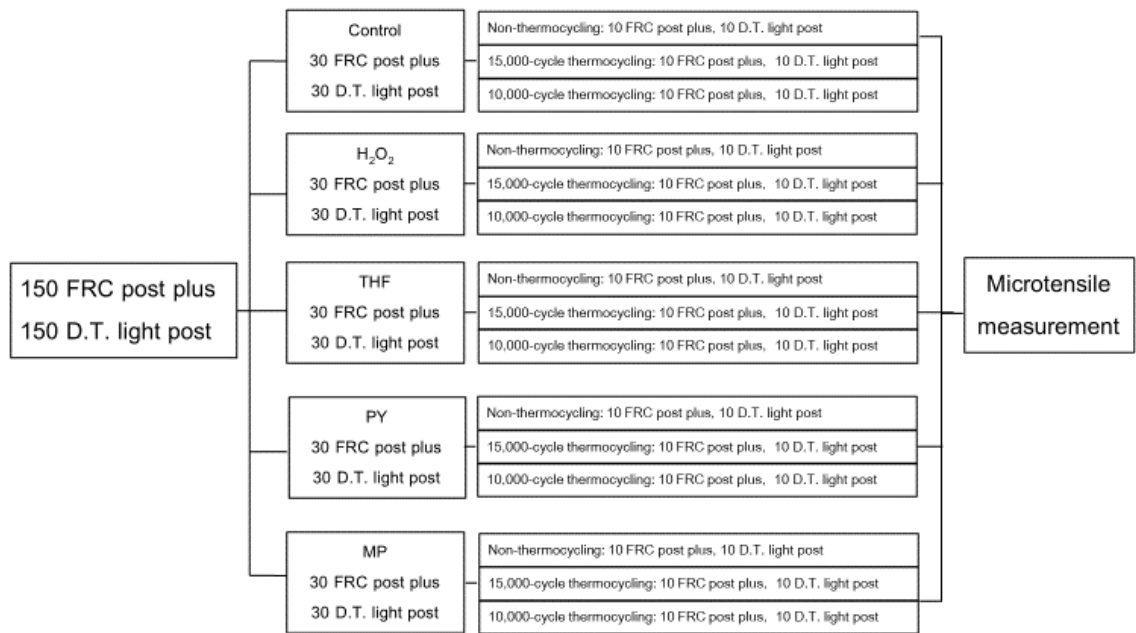


Figure 20 demonstrates schematic represent flow chart of specimen preparations.

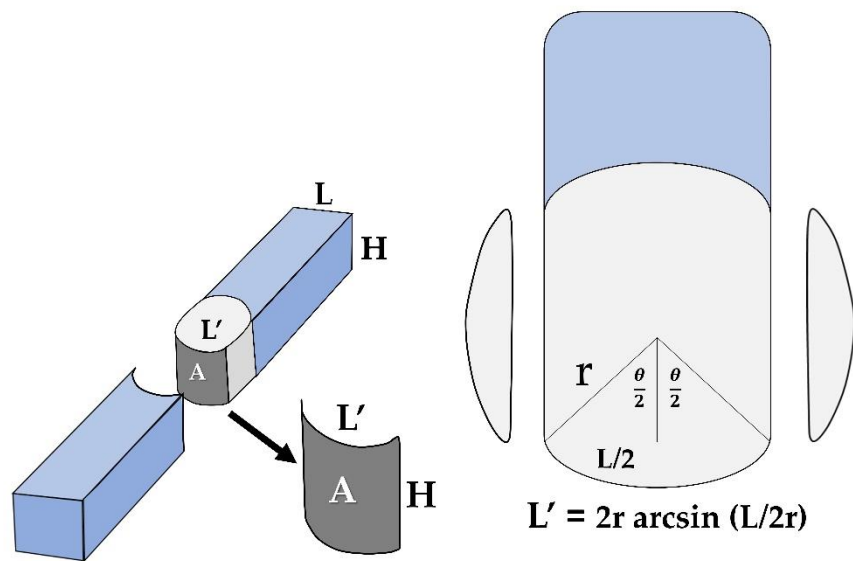


Figure 21 presents a graphic illustration of bond area calculation.

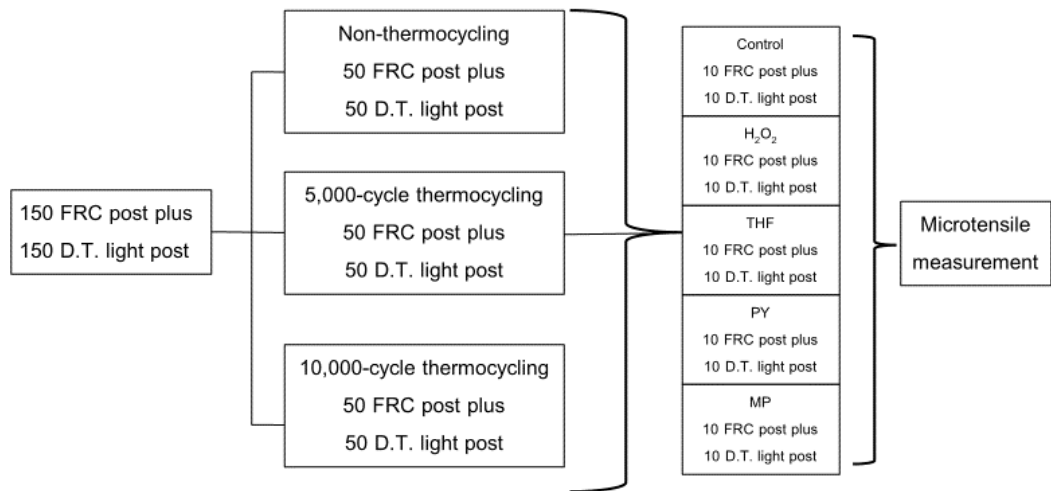


Figure 22 shows the schematic representation of all group specimens in the investigation.

3.4 Manufacturers and compositions of the materials are presented in Table 11. Table 11 exhibits trade names, manufacturers, and compositions of experimental materials.

Brand	Manufacturer	Composition
FRC post plus	Ivoclar Vivadent, Schaan, Liechtenstein	Glass fiber (61.5% w/w) Bis-EMA (10-13% w/w) ytterbium trifluoride (<10% w/w) Bis-GMA (3-7% w/w) 1,4-butanediol dimethacrylate (3-5% w/w)
D.T. light- post	Recherches Techniques Dentaires, RTD, St. Egreve, France	Epoxy resin matrix (40 vol%) Quartz fibers (60 vol%)

Multicore Flow	Ivoclar Vivadent, Schaan, Liechtenstein	Matrix: Bis-GMA, urethane dimethacrylate, triethylene glycol dimethacrylate, Fillers: barium glass, ytterbium Ba-Al-fluorosilicate glass, highly dispersed silicon dioxide. Particle size 0.04-25 μm Total volume of fillers (47%)
Excite F DSC	Ivoclar Vivadent, Schaan, Liechtenstein	Bis-GMA (25-30%), Ethanol (10-25%), 2-hydroxyethyl methacrylate (10-25%), phosphonic acid acrylate (10-25%), diphenyl (2,4,6-trimethylbenzoyl) phosphine oxide (<2.5%) potassium fluoride (<2.5%)
Monobond plus	Ivoclar Vivadent, Schaan, Liechtenstein	Ethanol, 3-(trimethoxysilyl)propyl methacrylate, methacrylated phosphoric acid ester
Tetrahydrofuran	LOBA Chemie Pvt. Ltd. - Jehangir Villa, 107, Wode House Road, Colaba, Mumbai, India	Tetrahydrofuran 99.8%
Hydrogen peroxide	LOBA Chemie Pvt. Ltd. - Jehangir Villa, 107,	Hydrogen peroxide 35%

	Wode House Road, Colaba, Mumbai, India	
Pyridine	LOBA Chemie Pvt. Ltd. - Jehangir Villa, 107, Wode House Road, Colaba, Mumbai, India	Pyridine 99.5%
Morpholine	LOBA Chemie Pvt. Ltd. - Jehangir Villa, 107, Wode House Road, Colaba, Mumbai, India	Morpholine 99.5%

3.5 Mode of failure evaluation

Stereo Microscope; SZ 61, Olympus, Tokyo, Japan. at 40x magnification was used to evaluate and classify the fracture area (adhesive, cohesive, mix).

The fracture area was calculated as a percentage of the total bonding area by taking use of the program Image J 1.41 (ImageJ 1.41, Wayne Rasband, National Institutes of Health, Bethesda, Maryland, United States), Cohesive failure was determined to be the mode of failure if the glass fiber post or composite core material interphase was found in more than 60 percent of the total bonding area. They were considered that is mixed failure if the percentage in this region is less than 60 percent but more than 40 percent. In addition, they are considered to have adhesive failure if the above regions composed less than 40 percent of the entire

3.6 Surface roughness measuring sample preparation.

3.6.1 Determination of Surface Properties with White Light Interferometry

Sample preparation materials

1. Glass fiber posts that would be measured.
2. Plastic mold with a hole on the holder, as shown in Figure 24.
3. Light curing flowable resin composite
4. A plate made of black acrylic resin in the shape of a rectangle, with a metal post and marker lines, as illustrated in Figure 25.

Step of sample preparation

1. The taper end of a fiber-reinforced composite post was placed 2 mm deep into a plastic mold.
2. A flowable resin composite was injected into the plastic mold and then activated with a light curing unit.
3. A plastic hole put into a metal post and attached to a post-plastic mold assembly linked a black acrylic resin plate to a glass fiber post-plastic mold assembly.
4. The assembled component was placed on the white light interferometry tester's stand.
5. On the surface of the fiber-reinforced composite posts that coincided to the marker line, the value of Ra was measured.
6. The sample from step 5 was submerged in a chemical solution for 1 minute before being rinsed with water and allowed to dry.
7. The surface roughness of the sample from step 6 was measured by repeating steps 3 to 5.
8. For each group, six samples were measured.

White light optical interferometry (WLI, ContourX-1000, Bruker, Salbruken, Germany) was employed to carry out the measurements, and a vertical scanning interferometry mode was utilized for the analysis (VSI). The field of view (FOV) was set to 0.55 degrees, and the magnification was set to 20, which resulted in an image size of 1.7 x 2.3 mm. Ra, which stands for the arithmetic mean height of surface, was included in the report.

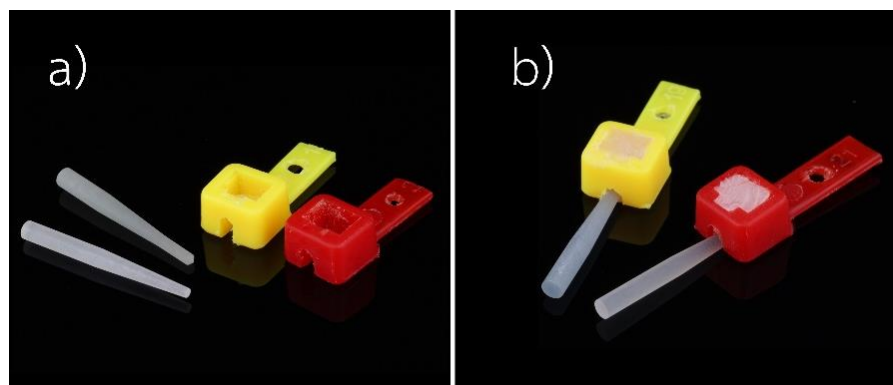


Figure 24 displays a) a glass fiber post, b) a plastic mold with a hole in the holder, and c) the insertion and attachment of the tapered end of the glass fiber posts in the plastic mold.

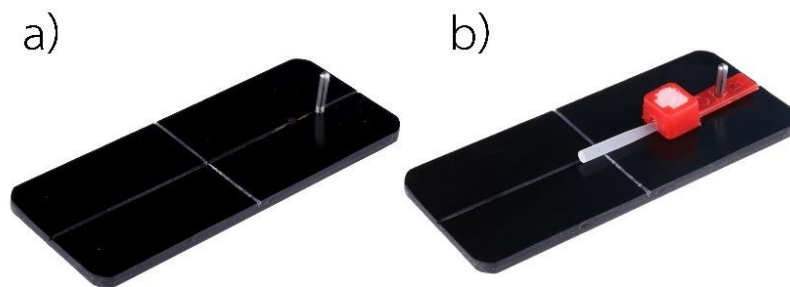


Figure 25 depicts a) a black acrylic resin plate with marker lines and a short metal post, and b) a glass fiber post-plastic mold assembly attached to the black acrylic resin plate.

3.6.2 Scanning electron microscope (SEM) evaluation

Two samples of each type of post received surface treatments were subjected to SEM for morphological analysis of the surface using a gold spotter coated (Gold sputtering unit, JEOL Ltd., Akishima, Japan) and then were observed through a scanning electron microscope (JSM-IT500HR, JEOL Ltd., Tokyo, Japan).

3.7 Sample size calculation

The sample size calculation was based on a 5% margin of error and 95% confidence level (significance of 0.05) using statistical software (G*Power v. 3.1.5, Faul, Erdfelder, Buchner and Lang, Heinrich Heine University, Düsseldorf, Germany, that can be downloaded from <http://www.gpower.hhu.de/en.html>) (168) and previous dental articles.

3.8 Statistical analysis

For the non-thermocycling, 5000-cycle, and 10,000-cycle thermocycling conditions, the data from each condition was analyzed using IBM SPSS Statistics for Windows version 22.0. The continuous outcome and normality of distribution of the

analyzed data were determined using a Kolmogorov–Smirnov test at a significance level of 0.05. Levene’s test was then used to analyze the equality of variation. The results showed that the data had a normal distribution and equal variance. Therefore, one-way analysis of variance (ANOVA) was used to analyze the data, followed by Tukey’s Honestly Significant Difference test ($p < 0.05$).

For the same chemical reagent treatment groups, an independent t-test was used to examine statistically significant differences ($p < 0.05$) between the D.T. Light-Post and FRC Postec Plus groups.

In white light interferometry surface roughness measurements, the mean surface roughness values of each type of post exhibited a normal distribution and equal variance. A one-way analysis of variance (ANOVA) was used to analyze the data, followed by Tukey’s Honestly Significant Difference test ($p < 0.05$).

3.9 Ethical considerations

No ethical consideration required.

CHAPTER 4

RESULTS

The microtensile bond strength

All the mean microtensile bond strength results are shown in Table 12, 13 and 14.

No thermocycling condition

In Bis-GMA resin matrix groups (FRC posts), the PY group exhibited the highest microtensile bond strength (41.09 ± 4.29), followed by MP group (34.44 ± 3.76), H₂O₂ group (31.15 ± 2.61), THF group (28.49 ± 1.86) and control group (29.64 ± 2.26), respectively. The microtensile bond strength of the PY group was significantly higher than that of the other groups. While the microtensile bond strength of the MP group was significantly higher than that of the THF, H₂O₂ and control groups. Moreover, the microtensile bond strength of the control group was not significantly different from that of the THF and H₂O₂ groups.

For epoxy resin matrix groups (D.T. light- posts), PY group showed the highest microtensile bond strength (46.93 ± 4.97), followed by THF group (40.73 ± 3.40), MP group (39.40 ± 2.80), H₂O₂ group (38.30 ± 3.16) and control group (33.22 ± 2.43), respectively. The microtensile bond strength of PY group showed significantly higher than that of the other groups. However, the microtensile bond strength of the THF, MP, and H₂O₂ group was considerably greater than that of the control group despite not being statistically different from one another.

In terms of the resin matrix type of glass fiber posts, the microtensile bond strength of epoxy resin matrix posts were significantly greater than that of Bis-GMA resin matrix posts across all intervention techniques.

Thermocycling condition

From the thermocycle testing, the 5,000-cycle thermocycling, in Bis-GMA resin matrix groups (FRC posts), the PY group exhibited the highest of microtensile bond strength (36.21 ± 5.39), followed by MP group (33.04 ± 4.43), H₂O₂ group (26.19 ± 2.36), THF group (26.31 ± 4.51) and control group (25.05 ± 4.71).

The PY group had the significantly highest microtensile bond strength of the other groups. The MP group was also significantly higher than that of the THF and control groups ($p < 0.05$). However, The MP group and H_2O_2 group was not significantly different from each other.

In the 5,000-cycle thermocycling, epoxy resin matrix groups (D.T. light- posts), the PY group demonstrated the highest of microtensile bond strength (41.96 ± 4.45), followed by MP group (34.80 ± 5.07), THF group (29.73 ± 4.60), H_2O_2 group (29.43 ± 3.58) and control group (27.81 ± 3.23), respectively. The microtensile bond strength of the PY group was significantly higher than that of the other groups. MP group was also significantly higher than control groups ($p < 0.05$). However, The MP, THF and H_2O_2 group was not significantly different from each other.

The Bis-GMA resin matrix groups (FRC posts) after 10000-cycle thermocycling, the PY group had the highest of microtensile bond strength (35.26 ± 3.65), followed by MP group (31.63 ± 4.97), H_2O_2 group (25.40 ± 2.18), THF group (25.59 ± 2.51) and control group (24.22 ± 4.07), consequently.

Similarly, to the previous result, the significant group with the highest microtensile bond strength was the PY group. MP group was significantly higher than that of the THF, H_2O_2 and control group ($p < 0.05$).

The 10,000-cycle thermocycling, for epoxy resin matrix groups (D.T. light-posts), the PY group displayed the highest of microtensile bond strength (39.76 ± 2.37), followed by MP group (31.42 ± 4.15), H_2O_2 group (28.84 ± 3.86), THF group (28.59 ± 3.17) and control group (26.33 ± 2.51).

The PY group had significantly higher microtensile bond strength than the other groups. However, the MP, THF and H_2O_2 groups were not significantly different from each other, and their microtensile bond strengths were significantly higher than of the control group ($p < 0.05$).

Table 12 shows the mean microtensile bond strength resulting from non-thermocycling conditions.

chemical agent type of resin matrix	Control	H ₂ O ₂ 35 % 60 s	THF 99.8% 60 s	Pyridine 99.5% 60 s	Morpholine 99.5% 60 s
Bis GMA (FRC post plus)	29.64±2.26c	31.15±2.61 bc	28.49±1.86 c	41.09±4.29 a	34.44±3.76b
Epoxy (D.T. light- post)	33.22 ±2.43c*	38.30±3.16 b*	40.73±3.40 b*	46.93±4.97 a*	39.40±2.80b*

Table 13 shows the mean microtensile bond strength resulting after 5,000-cycle thermocycling.

chemical agent type of resin matrix	Control	H ₂ O ₂ 35 % 60 s	THF 99.8% 60 s	Pyridine 99.5% 60 s	Morpholine 99.5% 60 s
Bis GMA (FRC post plus)	25.05±4.71c	26.19±2.36bc	26.31±4.51c	39.21±5.39a	33.04±4.43b
Epoxy (D.T. light- post)	27.81±3.23c	29.43±3.58bc	29.73±4.60bc	41.96±4.45a*	34.80±5.07b

Table 14 displays the mean microtensile bond strength obtained after 10,000-cycle thermocycling.

chemical agent type of resin matrix	Control	H ₂ O ₂ 35 % 60 s	THF 99.8% 60 s	Pyridine 99.5% 60 s	Morpholine 99.5% 60 s
Bis GMA (FRC post plus)	24.22±4.07c	25.40±2.18c	25.59±2.51c	35.26±3.65a	31.63±4.97b
Epoxy (D.T. light-post)	26.33±2.51c	28.84±3.86bc	28.59±3.17bc	39.76±2.37a*	31.42±4.15b

The failure modes

Tables 15–17 and Figures 26–28 illustrate the mode of failure of the non-thermocycling group, the 5,000-cycle and 10,000-cycle thermocycling groups.

Non thermocycling condition

It was shown in this study that higher adhesive failure was found in all groups, and mixed failure was also shown in all groups. Moreover, the highest percentages of mixed failure were demonstrated in the epoxy PY group. But cohesive failure was not found in any group.

5,000-cycle thermocycling condition

Higher adhesive failure mode was discovered in all groups. While mixed failure was also shown in all groups except Epoxy C, Bis-GMA PY, and Bis-GMA MP. For the cohesive failure mode, it was displayed only in the epoxy PY and Bis-GMA PY groups.

10,000-cycle thermocycling condition

It was observed that higher adhesive failure mode was found in all groups. While mixed failure was also shown in all groups except Epoxy H₂O₂, Epoxy MP and Bis-GMA H₂O₂. Furthermore, the cohesive failure mode was only seen in the epoxy PY group. It indicated a total of twenty percent.



Table 15 shows failure modes of non-thermocycling condition.

Group	Cohesive	Adhesive	Mixed
Epoxy C	0	80	20
Epoxy H ₂ O ₂	0	70	30
Epoxy THF	0	80	20
Epoxy PY	0	60	40
Epoxy MP	0	80	20
Bis-GMA C	0	80	20
Bis-GMA H ₂ O ₂	0	70	30
Bis-GMA THF	0	80	20
Bis-GMA PY	0	80	20
Bis-GMA MP	0	90	10

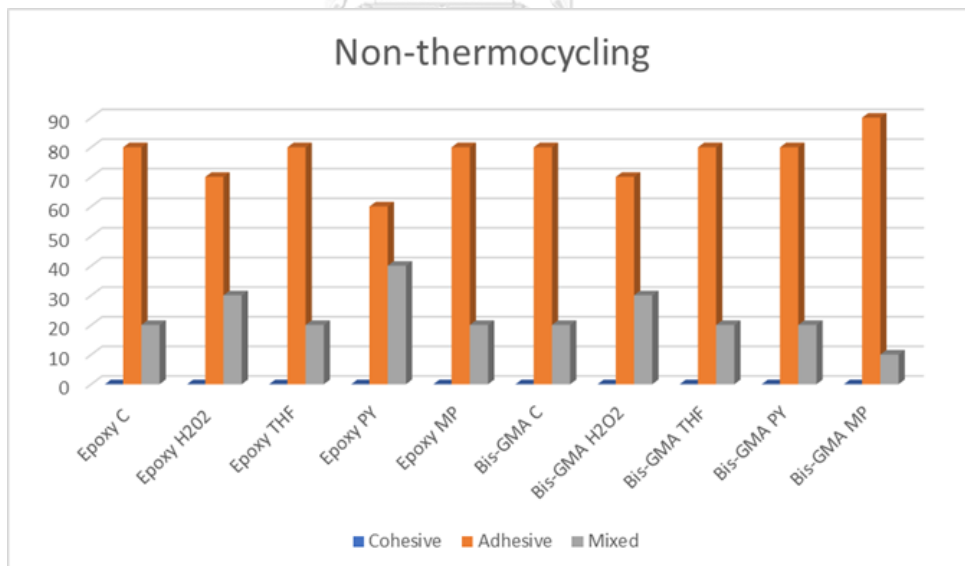


Figure 26 illustrate the bar graphs display the failure modes in the non-thermocycling condition.

Table 16 shows the failure modes of 5,000 thermocycling cycles.

Group	Cohesive	Adhesive	Mixed
Epoxy C	0	100	0
Epoxy H ₂ O ₂	0	90	10
Epoxy THF	0	90	10
Epoxy PY	10	80	10
Epoxy MP	0	90	10
Bis-GMA C	0	80	20
Bis-GMA H ₂ O ₂	0	80	20
Bis-GMA THF	0	90	10
Bis-GMA PY	10	90	0
Bis-GMA MP	0	100	0

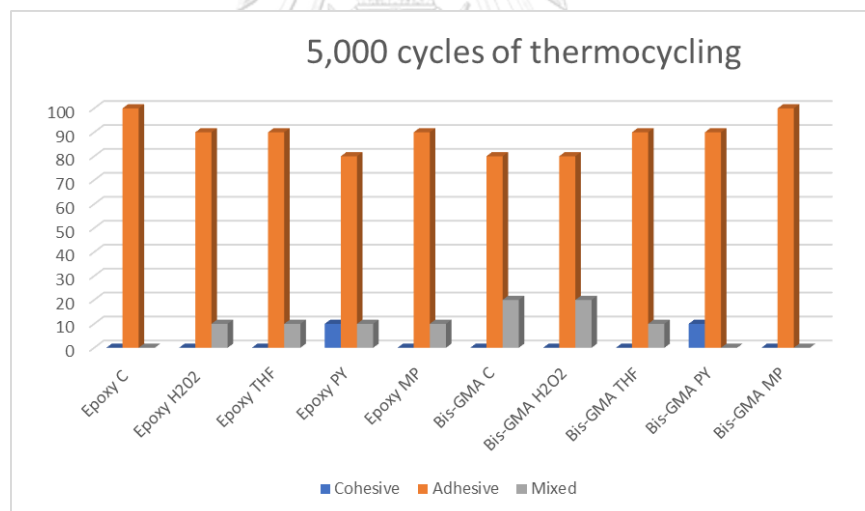


Figure 23 illustrate the bar graphs depict the failure modes after the 5,000-cycle thermocycling.

Table 17 shows the modes of failure resulting from 10,000-cycle thermocycling.

Group	Cohesive	Adhesive	Mixed
Epoxy C	0	100	0
Epoxy H ₂ O ₂	0	90	10
Epoxy THF	0	100	0
Epoxy PY	20	70	10
Epoxy MP	0	90	10
Bis-GMA C	0	100	0
Bis-GMA H ₂ O ₂	0	90	10
Bis-GMA THF	0	100	0
Bis-GMA PY	0	100	0
Bis-GMA MP	0	100	0

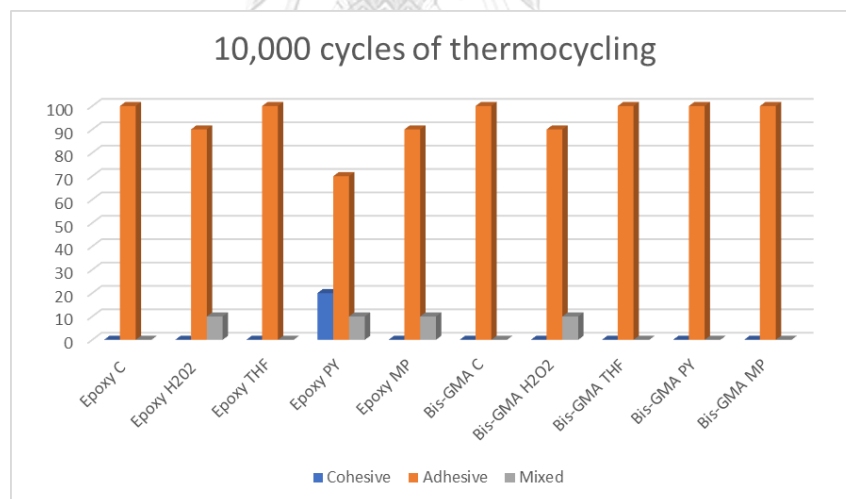


Figure 24 demonstrates the failure modes are shown by the bar graphs after 10,000-cycle thermocycling.

Surface roughness analysis results

- White Light Interferometry

The qualitative evaluations of roughness characteristics using white light interferometry are shown in Tables 18 and 19. In the Epoxy and Bis-GMA groups,

treatment with an aprotic solvent (THF, PY, and MP) significantly decreased Ra relative to each control group. Table 18 shows the surface roughness (Ra) of Epoxy groups using white light interferometry.

Group	Ra (μm)
Epoxy C	514.860 \pm 31.801c
Epoxy H ₂ O ₂	596.661 \pm 32.910b
Epoxy THF	614.874 \pm 36.120b
Epoxy PY	704.140 \pm 44.637a
Epoxy MP	664.629 \pm 37.545ab

Table 19 displays the surface roughness (Ra) of Bis-GMA groups. using white light interferometry.

Group	Ra (μm)
Bis-GMA C	584.970 \pm 22.221b
Bis-GMA H ₂ O ₂	585.884 \pm 31.036b
Bis-GMA THF	608.670 \pm 36.106b
Bis-GMA PY	859.439 \pm 30.789a
Bis-GMA MP	621.812 \pm 41.610b

- Scanning Electron Microscope (SEM)

The SEM result showed that fibers glass or quartz were not damaged by all treatment agents. Their results revealed that all treatment can differently alter the surface topography of both epoxy and Bis-GMA resin matrix as displayed in Figure 29-30.

Pyridine application can result in more removal of both resin matrixes than other treatments in both the epoxy (D.T. light-post) and Bis-GMA (FRC post plus)

matrixes, which can expose more surface fibers. While tetrahydrofuran slightly removes Bis-GMA resin matrix when compared to others as shown in Figure 30.

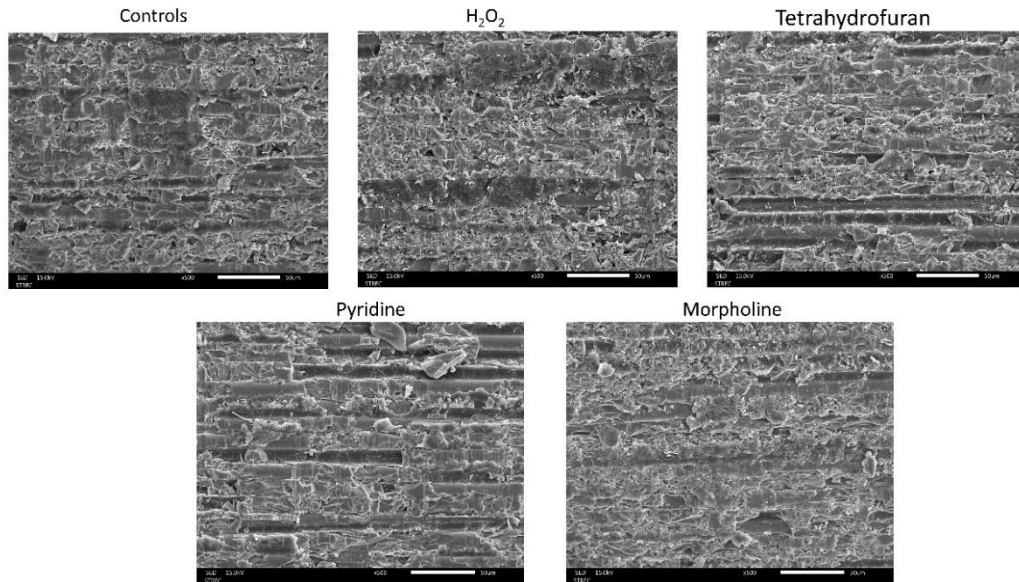


Figure 25 demonstrates the surface topography of Epoxy (D.T. light-post) control and treatment groups, which are hydrogen peroxide, tetrahydrofuran, pyridine, and morpholine, for 1 minute.

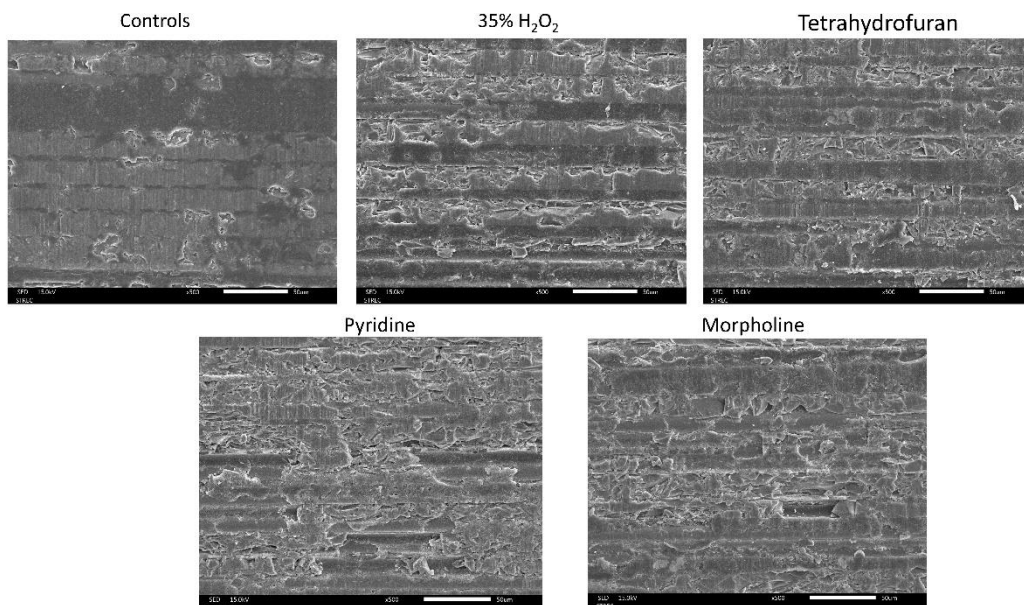


Figure 26 represents the surface topography of Bis-GMA (FRC post plus) control and treatment groups, which are hydrogen peroxide, tetrahydrofuran, pyridine, and morpholine, for 1 minute.

CHAPTER 5

DISCUSSION

Endodontically treated teeth are typically severely damaged by caries, excessive wear, previous restorative treatment, or endodontic procedures leading to a lack of coronal tooth structure. In these clinical conditions, cast metal posts and cores have historically been employed to provide the essential retention for eventual prosthetic rehabilitation. Fiber-reinforced composite posts were launched in the 1990s as a replacement for traditional custom-made cast posts and prefabricated metal posts. Dental fiber-reinforced composite posts have been widely used in endodontically treated teeth. Because of the similarities in elastic modulus with dentin, they have been shown to outperform cast metal posts. While abutment build-up around a fiber post is essential when there is considerable loss of coronal tooth structure (169). For core build-up material, resin composite is a material of choice for use with fiber-reinforced composite posts due to its hardness and fracture toughness resemblance to tooth structure, allowing for preparation after curing. When utilized to perform core restorations, they must produce good outcomes in terms of microscopic structural integrity as well as surface adaptability surrounding fiber posts (24, 38, 41, 170, 171). The bonding ability of the core material and the fiber post is a key component influencing the final restoration survival rate (172, 173).

Therefore, the purpose of this study was to investigate the effect of aprotic solvents on the polymer covering the fiber post surface. The results of the study revealed that the microtensile bond strength of fiber-reinforced composite posts varied significantly between testing groups and resin matrix types. Therefore, the null hypothesis was rejected.

The microtensile bond test, which is performed in the current investigation, is characterized using specimens with tiny bonding regions. (less than 2 mm²), which lessens the chance of defects (defects) that impair the bond and increases data variation (174). Moreover, Due to axial tensile loading on a smaller contact, the microtensile test permits a more uniform stress distribution than the shear bond strength test. As a result, there are less cohesive fractures (175). In addition,

microtensile testing produces more trustworthy results and can be used to relatively small samples (176, 177).

In a number of studies, researchers came to the conclusion that premature bond failure, which had an effect on the bond strength value, was associated to cutting procedures that induced higher mechanical stress at the interface. This was in addition to experimental variables such as cutting speed and specimen shape, as well as by intrinsic material properties (178, 179). The decision to exclude from statistical analysis would result in underestimation of the mean bond strength values (180).

In our investigation, the number of premature failures before or after thermocycling was less than 2%, so we chose to omit the premature failure specimens. As a result, there was no zero in any of the specimens. For the bonding area configuration, the post- resin composite core contact was curved. Therefore, the area measurement calculation was modified. $A = 2r \arcsin (L/2r) \times h$, where r , L , and h were the diameter, width, and height of the post, respectively (45, 181).

Hydrogen peroxide is an alkaline chemical that, through a substrate oxidation process involving the electrophilic attack of hydrogen peroxide on the cured secondary amine, can only partially dissolve the epoxy resin matrix (34, 57, 182).

The effect of different hydrogen peroxide concentrations and application periods on fiber posts was studied. The concentrations of 10% (48), 20% (49), 24% (60, 183), 35% (183, 184) and 50% (60) were taken into treatment fiber post surface study. However, regardless of application time, bond strength was not different between 50% and 24% hydrogen peroxide (60). When comparing 24% to 35% hydrogen peroxide, the study found that when the solutions were applied over the post surface or by immersion, the bond strength of 35% hydrogen peroxide was stronger than that of 24% (183). For the application time of 24% and 35% concentrations, the bond strength of 1 minute was not significantly different from that of 5 and 10 minutes. Furthermore, as compared to 15 second, 30 second, and control groups, the application duration of 35% concentration in 1 minute revealed the strongest bond strength (185). As a consequence, this study utilized hydrogen peroxide at a concentration of 35% for an application period of 1 minute by

immersion, which was simpler to control in the experiments, and extended this technique to other surface treatment groups.

Tetrahydrofuran, pyridine, and morpholine were used as aprotic solvents in this investigation. The microtensile bond result revealed that an aprotic solvent can boost the microtensile bond strength more than hydrogen peroxide at the same application time. This would imply that the peroxide's oxidation effect left residual oxygen in the post-surface (183, 184), which could then affect the polymerization process (186), which exhibited the microtensile bond strength before and after thermocycling.

Existing data about the influence of an aprotic solvent on the surface treatment of fiber-reinforced composite posts is limited. It is commonly acknowledged that a solvent is acceptable for dissolving a polymer if their solubility properties are comparable. The closer the similarity between the solute and solvent solubility parameters, the higher the likelihood that the solute will be soluble in the particular solvent (115). Consequently, solubility parameters, a numerical number reflecting the relative solubility characteristics of a single solvent, are one of the most important criteria in selecting a solvent for applications. For a dimethacrylate polymer such as Bis-GMA, it has a solubility parameter of $22.13 \text{ (MPa)}^{1/2}$ (187), while epoxy resin has $23.75 \text{ (MPa)}^{1/2}$ (14). Whereas aprotic solvents have the following solubility parameters: tetrahydrofuran $19.4 \text{ (MPa)}^{1/2}$, pyridine $21.8 \text{ (MPa)}^{1/2}$, and morpholine $21.5 \text{ (MPa)}^{1/2}$ (14). However, not only solubility parameter but also other factors such as concentration, temperature, application duration, and pH impact the effectiveness of an aprotic solvent (188).

In this present study, we found high bond strength in both the non-protic and aprotic solvent groups. This could be due to bonding between the bonding agent and the rein matrix, as well as between the bonding agent and the fiber-reinforced fiber.

For quartz or glass fibers, the purpose of the surface treatment of fiber-reinforced composite post was to remove the resin matrix on the surface layer, exposing more quartz or glass fibers to produce a chemical bond interaction

between silane coupling agents and hydroxy groups on the glass/quartz surface. This chemical bond has a greater impact on bond strength.

Especially, the pyridine treated epoxy resin matrix group showed the highest microtensile bond strength. This could be explained by the fact that the pyridine and epoxy resin matrices of glass/quartz fiber posts have a closed solubility parameter. As a result, pyridine can dissolve and swell the epoxy resin matrix, resulting in two processes for improving the bond strength between fiber-reinforced composite post and resin core build up material.

1. The resin matrix covering the glass fiber was dissolved and removed, exposing the glass fiber. In this regard, the fibers are composed of hydroxyl group, which can be silanated to create enough adhesion to the bonding agent.

2. When the resin matrix was dissolved and swelled. There are two possibilities for obtaining adhesion between the polymer matrix and the new bonding resin.

- 2.1 Mechanical interlocking caused by rough surfaces.

- 2.2 Adhesion by interpenetrating network (IPN) formation, When the resin matrix swelled and became soft and created the pores between polymer chains, it permitted the transfer of low-molecular-weight monomers from the bonding agent to diffusion into the swelled polymer matrix. The adhesion was accomplished after curing through IPN production.

In this study, we chose white Light Interferometry for surface roughness measurement because it is a non-contact optical method for 3D-profiles of rough and smooth surfaces (154, 155, 156).

As a result, we can use the same specimens to measure roughness before and after surface treatment, providing more trustworthy results. Therefore, we can use the same specimens for measurement the roughness before and after surface treatment this would give more reliable data. For the SEM investigation, the results demonstrate changes in surface topography in all treated surface groups, as illustrated in Figures 22-26. They had more exposed glass fiber than the control group.

For the mode of failure, debonding of a resin composite core of the fiber post happens frequently at the contact between these two components. It has an

impact on the quality of prosthesis. As a result, the adhesion between post and core restorative materials is critical (113). There are two adherend surfaces adhered by the resin composite can be deboned either by “cohesive” or “adhesive” failure (2). Cohesive failure occurs in the bulk region of resin matrix of fiber-reinforced composite post or in the bulk of an adherend resin composite core material. Adhesive failure, on the other hand, occurs at the contact between a fiber-reinforced composite post and an attached resin composite material.

Mixed failure happens because of a combination of cohesive and adhesive modes. In general, the cohesive mode is preferable to achieve a relatively high adhesive strength. If the bond strength between the resin composite core material and the adhering surface is insufficient, adhesive failure takes place, leading to facile debonding. In this study, it was found that there was no cohesive failure in non-thermocycling groups and increasing cohesive failure only PY groups in 5,000 and 10,000-cycle thermocycling. Which means that PY group has a high adhesive strength.

The relation of thermocycling and mode of failure, thermocycling is employed to weaken by aging a bonding interphase and resin composite (2, 189). In this study, 5,000 and 10,000-cycle thermocycling at 5C° and 55C° were used to simulate a six-month and one-year longevity in an oral environment, respectively (190).

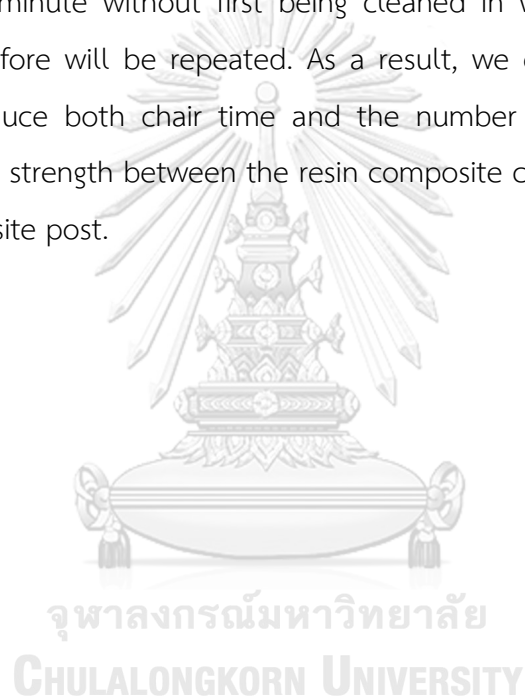
In addition to decreasing the physicochemical qualities of composite resin, changes in temperature can also reduce the quantity of unreacted double bonds (191). Regarding to 5,000 and 10,000-cycle thermocycling, all cohesive failure was occurred in post interphase, this result may imply to research which report that the mechanical property of fiber-reinforced composite post after thermocycling was decreased, so the weakest was in fiber-reinforced composite post interphase as shown in cohesive failure appearance.

After being subjected to thermocycling, the discrepancies in the coefficients of thermal expansion (CTE) of each of the components may be responsible for the decrease in the micro tensile strength (192, 193).

Additionally, there is the possibility that void space inside the resin matrix could promote water absorption, which will lead to a decrease in the flexural strength of the fiber-reinforced composite post (194).

In this experiment, the specimens were submerged in solution for one minute before being washed with water for one minute. The treated specimens were subsequently treated with a silane coupling agent, bonding agent, and placed in a silicone mold filled with resin composite core build-up materials.

In a subsequent investigation, the specimens will be submerged with the solution for one minute without first being cleaned in water. Following that, the process stated before will be repeated. As a result, we expect that the reduction approach will reduce both chair time and the number of working steps without affecting the bond strength between the resin composite core material and the fiber-reinforced composite post.



CHAPTER 6

CONCLUSION

From the limitations of this study, it can be concluded that.

- 1) As aprotic solvents, pyridine can increase the highest microtensile bond strength between the interphase of composite core and fiber-reinforced composite post both Bis-GMA (FRC post plus) and epoxy resin matrix (D.T. light-post). Moreover, pyridine is more effective with epoxy resin than with bis-GMA resin.
- 2) As a result of surface roughness analysis pyridine can increase the highest surface roughness.
- 3) The thermocycling process decreased the microtensile bond strength of all groups, but the pyridine groups had the highest bonds.

REFERENCES

1. Monticelli F, Osorio R, Sadek FT, Radovic I, Toledano M, Ferrari M. Surface treatments for improving bond strength to prefabricated fiber posts: a literature review. *Oper Dent*. 2008;33(3):346-55.
2. Hayashi M, Ebisu S. Key factors in achieving firm adhesion in post-core restorations. *Japanese Dental Science Review*. 2008;44:22-8.
3. Goracci C, Raffaelli O, Monticelli F, Balleri B, Bertelli E, Ferrari M. The adhesion between prefabricated FRC posts and composite resin cores: microtensile bond strength with and without post-silanization. *Dent Mater*. 2005;21(5):437-44.
4. Schmage P, Cakir FY, Nergiz I, Pfeiffer P. Effect of surface conditioning on the retentive bond strengths of fiberreinforced composite posts. *J Prosthet Dent*. 2009;102(6):368-77.
5. Prado M, Marques JN, Pereira GD, da Silva EM, Simão RA. Evaluation of different surface treatments on fiber post cemented with a self-adhesive system. *Mater Sci Eng C Mater Biol Appl*. 2017;77:257-62.
6. Yenisey M, Kulunk S. Effects of chemical surface treatments of quartz and glass fiber posts on the retention of a composite resin. *J Prosthet Dent*. 2008;99(1):38-45.
7. Akin GE, Akin H, Sipahi C, Piskin B, Kirmali O. Evaluation of surface roughness and bond strength of quartz fiber posts after various pre-treatments. *Acta Odontol Scand*. 2014;72(8):1010-6.
8. Mazzitelli C, Ferrari M, Toledano M, Osorio E, Monticelli F, Osorio R. Surface roughness analysis of fiber post conditioning processes. *J Dent Res*. 2008;87(2):186-90.
9. Sumitha M, Kothandaraman R, Sekar M. Evaluation of post-surface conditioning to improve interfacial adhesion in post-core restorations. *J Conserv Dent*. 2011;14(1):28-31.
10. Monticelli F, Toledano M, Tay FR, Cury AH, Goracci C, Ferrari M. Post-surface conditioning improves interfacial adhesion in post/core restorations. *Dent Mater*. 2006;22(7):602-9.
11. Caravati EM. Acute hydrofluoric acid exposure. *Am J Emerg Med*. 1988;6(2):143-

- 50.
12. Watt BE, Proudfoot AT, Vale JA. Hydrogen peroxide poisoning. *Toxicol Rev.* 2004;23(1):51-7.
13. Monticelli F, Osorio R, Toledano M, Goracci C, Tay FR, Ferrari M. Improving the quality of the quartz fiber postcore bond using sodium ethoxide etching and combined silane/adhesive coupling. *J Endod.* 2006;32(5):447-51.
14. Hansen CM. HANSEN SOLUBILITY PARAMETERS: A User's Handbook. 2nd ed. Boca Raton: CRC press; 2007.
15. Gonçalves AP, Ogliari Ade O, Jardim Pdos S, Moraes RR. Chemical cleaning agents and bonding to glass-fiber posts. *Braz Oral Res.* 2013;27(1):70-2.
16. Fontes ST, Fernández MR, Ogliari FA, de Carvalho RV, de Moraes RR, Pinto MB, et al. Tetrahydrofuran as solvent in dental adhesives: cytotoxicity and dentin bond stability. *Clin Oral Investig.* 2013;17(1):237-42.
17. Glazer B. Restoration of endodontically treated teeth with carbon fibre posts--a prospective study. *J Can Dent Assoc.* 2000;66(11):613-8.
18. Goracci C, Ferrari M. Current perspectives on post systems: a literature review. *Aust Dent J.* 2011;56 Suppl 1:77-83.
19. Wolff D, Geiger S, Ding P, Staehle HJ, Frese C. Analysis of the interdiffusion of resin monomers into pre-polymerized fiber-reinforced composites. *Dent Mater.* 2012;28(5):541-7.
20. Dietschi D, Ardu S, Rossier-Gerber A, Krejci I. Adaptation of adhesive post and cores to dentin after in vitro occlusal loading: evaluation of post material influence. *J Adhes Dent.* 2006;8(6):409-19.
21. Bateman G, Ricketts DN, Saunders WP. Fibre-based post systems: a review. *Br Dent J.* 2003;195(1):43-8; discussion 37.
22. Wang Z, Ji Y, Zhang F. Bond strengths of an epoxy resin-based fiber post with four adhesive systems. *Quintessence Int.* 2010;41(9):e173-80.
23. Hedlund SO, Johansson NG, Sjögren G. A retrospective study of pre-fabricated carbon fibre root canal posts. *J Oral Rehabil.* 2003;30(10):1036-40.
24. Cagidiaco MC, Radovic I, Simonetti M, Tay F, Ferrari M. Clinical performance of fiber post restorations in endodontically treated teeth: 2-year results. *Int J Prosthodont.*

2007;20(3):293-8.

25. Soares CJ, Santana FR, Pereira JC, Araujo TS, Menezes MS. Influence of airborne-particle abrasion on mechanical properties and bond strength of carbon/epoxy and glass/bis-GMA fiber-reinforced resin posts. *J Prosthet Dent.* 2008;99(6):444-54.
26. Ferrari M, Vichi A, Mannocci F, Mason PN. Retrospective study of the clinical performance of fiber posts. *Am J Dent.* 2000;13(Spec No):9b-13b.
27. Lassila LV, Vallittu PK. The effect of fiber position and polymerization condition on the flexural properties of fiber-reinforced composite. *J Contemp Dent Pract.* 2004;5(2):14-26.
28. Lamichhane A, Xu C, Zhang FQ. Dental fiber-post resin base material: a review. *J Adv Prosthodont.* 2014;6(1):60-5.
29. Monticelli F, Toledano M, Tay FR, Sadek FT, Goracci C, Ferrari M. A simple etching technique for improving the retention of fiber posts to resin composites. *J Endod.* 2006;32(1):44-7.
30. Asmussen E, Peutzfeldt A. Influence of UEDMA BisGMA and TEGDMA on selected mechanical properties of experimental resin composites. *Dent Mater.* 1998;14(1):51-6.
31. Bell AM, Lassila LV, Kangasniemi I, Vallittu PK. Bonding of fibre-reinforced composite post to root canal dentin. *J Dent.* 2005;33(7):533-9.
32. Daneshkazemi A, Davari A, Askari N, Kaveh M. Effect of different fiber post surface treatments on microtensile bond strength to composite resin. *J Prosthet Dent.* 2016;116(6):896-901.
33. Elnaghy AM, Elsaka SE. Effect of surface treatments on the flexural properties and adhesion of glass fiber-reinforced composite post to self-adhesive luting agent and radicular dentin. *Odontology.* 2016;104(1):60-7.
34. Baskin DG, Erlandsen SL, Parsons JA. Influence of hydrogen peroxide or alcoholic sodium hydroxide on the immunocytochemical detection of growth hormone and prolactin after osmium fixation. *J Histochem Cytochem.* 1979;27(9):1290-2.
35. Combe EC, Shaglouf AM, Watts DC, Wilson NH. Mechanical properties of direct core build-up materials. *Dent Mater.* 1999;15(3):158-65.
36. Assif D, Oren E, Marshak BL, Aviv I. Photoelastic analysis of stress transfer by endodontically treated teeth to the supporting structure using different restorative

techniques. *J Prosthet Dent.* 1989;61(5):535-43.

37. Ahn S-G, Sorensen J. Comparison of mechanical properties of various post and core materials. *J Korean Acad Prosthodont.* 2002;41.

38. Panitiwat P, Salimee P. Effect of different composite core materials on fracture resistance of endodontically treated teeth restored with FRC posts. *J Appl Oral Sci.* 2017;25(2):203-10.

39. Ferracane JL. Resin composite--state of the art. *Dent Mater.* 2011;27(1):29-38.

40. El-Sahn NA, El-Kassas DW, El-Damanhoury HM, Fahmy OM, Gomaa H, Platt JA. Effect of C-factor on microtensile bond strengths of low-shrinkage composites. *Oper Dent.* 2011;36(3):281-92.

41. Spinhayer L, Bui ATB, Leprince JG, Hardy CMF. Core build-up resin composites: an in-vitro comparative study. *Biomater Investig Dent.* 2020;7(1):159-66.

42. Naumann M, Sterzenbach G, Rosentritt M, Beuer F, Frankenberger R. In vitro performance of self-adhesive resin cements for post-and-core build-ups: influence of chewing simulation or 1-year storage in 0.5% chloramine solution. *Acta Biomater.* 2010;6(11):4389-95.

43. Naumann M, Sterzenbach G, Rosentritt M, Beuer F, Meyer-Lückel H, Frankenberger R. Self-adhesive cements as core build-ups for one-stage post-endodontic restorations? *Int Endod J.* 2011;44(3):195-202.

44. Kim YH, Lee JH. Influence of modification in core building procedure on fracture strength and failure patterns of premolars restored with fiber post and composite core. *J Adv Prosthodont.* 2012;4(1):37-42.

45. Valandro LF, Yoshiga S, de Melo RM, Galhano GA, Mallmann A, Marinho CP, et al. Microtensile bond strength between a quartz fiber post and a resin cement: effect of post surface conditioning. *J Adhes Dent.* 2006;8(2):105-11.

46. Sahafi A, Peutzfeld A, Asmussen E, Gotfredsen K. Effect of surface treatment of prefabricated posts on bonding of resin cement. *Oper Dent.* 2004;29(1):60-8.

47. Sahafi A, Peutzfeldt A, Asmussen E, Gotfredsen K. Bond strength of resin cement to dentin and to surface-treated posts of titanium alloy, glass fiber, and zirconia. *J Adhes Dent.* 2003;5(2):153-62.

48. Vano M, Goracci C, Monticelli F, Tognini F, Gabriele M, Tay FR, et al. The

- adhesion between fibre posts and composite resin cores: the evaluation of microtensile bond strength following various surface chemical treatments to posts. *Int Endod J*. 2006;39(1):31-9.
49. Mosharraf R, Ranjbarian P. Effects of post surface conditioning before silanization on bond strength between fiber post and resin cement. *J Adv Prosthodont*. 2013;5(2):126-32.
50. Urban MV, Rath T, Radtke C. Hydrogen peroxide (H₂O₂): a review of its use in surgery. *Wien Med Wochenschr*. 2019;169(9-10):222-5.
51. Zhu G, Wang Q, Lu S, Niu Y. Hydrogen Peroxide: A Potential Wound Therapeutic Target? *Med Princ Pract*. 2017;26(4):301-8.
52. Johansson I, Somasundaran P. Handbook for cleaning/decontamination of surfaces 2007.
53. Fowles J, Boatman R, Bootman J, Lewis C, Morgott D, Rushton E, et al. A review of the toxicological and environmental hazards and risks of tetrahydrofuran. *Crit Rev Toxicol*. 2013;43(10):811-28.
54. Aguinaco A, Pocostales P, García-Araya J, Beltrán F. Decomposition of hydrogen peroxide in the presence of activated carbons with different characteristics. *Journal of Chemical Technology and Biotechnology*. 2011;86:595-600.
55. Brorson SH, Hansen AR, Nielsen HZ, Woxen IK. A comparative study of the immunogold labeling on H₂O₂-treated and heated epoxy sections. *Micron*. 2001;32(2):147-51.
56. Murphy MP, Bayir H, Belousov V, Chang CJ, Davies KJA, Davies MJ, et al. Guidelines for measuring reactive oxygen species and oxidative damage in cells and in vivo. *Nat Metab*. 2022;4(6):651-62.
57. Sloan FE. Chemical Attack of Graphite/Epoxy by Hydrogen Peroxide. *Applied Spectroscopy*. 1992;46(3):524-8.
58. Holm R, Farrants GW, Nesland JM, Sobrinho-Simões M, Jørgensen OG, Johannessen JV. Ultrastructural and electron immunohistochemical features of medullary thyroid carcinoma. *Virchows Arch A Pathol Anat Histopathol*. 1989;414(5):375-84.
59. Eneström S, Kniola B. Resin embedding for quantitative immunoelectron

- microscopy. A comparative computerized image analysis. *Biotech Histochem.* 1995;70(3):135-46.
60. de Sousa Menezes M, Queiroz EC, Soares PV, Faria-e-Silva AL, Soares CJ, Martins LR. Fiber post etching with hydrogen peroxide: effect of concentration and application time. *J Endod.* 2011;37(3):398-402.
61. PubChem. PubChem Compound Summary for CID 8028, Tetrahydrofuran Bethesda (MD): National Library of Medicine (US), National Center for Biotechnology Information; 2004 [Available from: <https://pubchem.ncbi.nlm.nih.gov/compound/Tetrahydrofuran>].
62. Bowron DT, Finney JL, Soper AK. The structure of liquid tetrahydrofuran. *J Am Chem Soc.* 2006;128(15):5119-26.
63. Wang Y, Zhao D, Rodríguez-Padrón D, Len C. Recent Advances in Catalytic Hydrogenation of Furfural. *Catalysts.* 2019;9(10):796.
64. Merat N, Godawa C, Gaset A. High selective production of tetrahydrofurfuryl alcohol: Catalytic hydrogenation of furfural and furfuryl alcohol. *Journal of Chemical Technology & Biotechnology.* 1990;48(2):145-59.
65. Dawes G, Scott E, Nötre J, Sanders J, Bitter JH. ChemInform Abstract: Deoxygenation of Biobased Molecules by Decarboxylation and Decarbonylation — A Review on the Role of Heterogeneous, Homogeneous and Bio-Catalysis. *Green Chem.* 2015;17.
66. Cai C, Kumar R, Zhang T, Wyman C. THF co-solvent enhances hydrocarbon fuel precursor yields from lignocellulosic biomass. *Green Chemistry.* 2013;15:3140-5.
67. Queyroy S, Müller-Plathe F. Molecular dynamics simulation of liquid tetrahydrofuran: On the uniqueness of force fields. *Molecular Physics*, v101, 779-787 (2003). 2003;101.
68. Roggendorf E, Spatz R. Systematic use of tetrahydrofuran in reversed-phase high-performance liquid chromatography: An example of the selectivity benefits of ternary mobile phases. *Journal of Chromatography A.* 1981;204:263-8.
69. Horváth P, Gergely A, Mazák K, Kökösi J, Szász G. Novel Data on the Effect of Tetrahydrofuran as an Organic Co-Modifier in RP-HPLC. *Chromatographia.* 2013;76.

70. Li AC, Li Y, Guirguis MS, Caldwell RG, Shou WZ. Advantages of using tetrahydrofuran-water as mobile phases in the quantitation of cyclosporin A in monkey and rat plasma by liquid chromatography-tandem mass spectrometry. *J Pharm Biomed Anal.* 2007;43(1):277-84.
71. Wiesenthal KE, Suffet IH. The effect of white or grey PVC pipe and its joint solvents (primer and cement) on odour problems in drinking water distribution systems. *Water Sci Technol.* 2007;55(5):169-76.
72. Luque-Agudo V, Gallardo-Moreno AM, González-Martín ML. Influence of Solvent and Substrate on Hydrophobicity of PLA Films. *Polymers (Basel).* 2021;13(24).
73. Fontes ST, Ogliari FA, Lima GS, Bueno M, Schneider LF, Piva E. Tetrahydrofuran as alternative solvent in dental adhesive systems. *Dent Mater.* 2009;25(12):1503-8.
74. Kourounakis AP, Xanthopoulos D, Tzara A. Morpholine as a privileged structure: A review on the medicinal chemistry and pharmacological activity of morpholine containing bioactive molecules. *Med Res Rev.* 2020;40(2):709-52.
75. Palchykov V. Morpholines. Synthesis and Biological Activity. *Russian Journal of Organic Chemistry.* 2013;49.
76. Wijtmans R, Vink MKS, Schoemaker HE, Delft FL, Blaauw R, Rutjes F. Biological relevance and synthesis of C-substituted morpholine derivatives. *Synthesis.* 2004:641-62.
77. Zhao J, Liu H, Chen W, Jian Y, Zeng G, Wang Z. Hydrogel of HEMA, NVP, and Morpholine-Derivative Copolymer for Sulfate Ion Adsorption: Behaviors and Mechanisms. *Molecules.* 2023;28(3).
78. PubChem. PubChem Compound Summary for CID 8083, Morpholine Bethesda (MD): National Library of Medicine (US), National Center for Biotechnology Information 2004 [Available from: <https://pubchem.ncbi.nlm.nih.gov/compound/Morpholine>].
79. Some organic solvents, resin monomers and related compounds, pigments and occupational exposures in paint manufacture and painting. *IARC Monogr Eval Carcinog Risks Hum.* 1989;47:1-442.
80. Kozin VG, Mukhamadiev AA. Dissolving and Selective Properties of Morpholine-based Mixed Solvents. *Russian Journal of Applied Chemistry.* 2001;74(8):1289-94.
81. Kumari A, Singh RK. Morpholine as ubiquitous pharmacophore in medicinal

chemistry: Deep insight into the structure-activity relationship (SAR). *Bioorg Chem.* 2020;96:103578.

82. Cao P, Chen DW, Liang J, Wu PG, Wen S, Wei J, et al. Concentration of morpholine residues in major fruits and juices and its dietary exposure in China. *Food Addit Contam Part A Chem Anal Control Expo Risk Assess.* 2019;36(1):26-34.
83. Johnson RS. Final report on the safety assessment of Cetethyl Morpholinium Ethosulfate. *Int J Toxicol.* 2001;20 Suppl 3:99-102.
84. Ghafary S, Ranjbar S, Larijani B, Amini M, Biglar M, Mahdavi M, et al. Novel morpholine containing cinnamoyl amides as potent tyrosinase inhibitors. *Int J Biol Macromol.* 2019;135:978-85.
85. Harbison RD, Marino DJ, Conaway CC, Rubin LF, Gandy J. Chronic morpholine exposure of rats. *Fundam Appl Toxicol.* 1989;12(3):491-507.
86. Klaisiri A, Suebnukarn S, Krajangta N, Rakmanee T, Sriamporn T, Thamrongananskul N. The Effect of Morpholine on Composite-to-Composite Repair Strength Contaminated with Saliva. *Polymers.* 2022;14(21):4718.
87. PubChem. PubChem Compound Summary for CID 1049, Pyridine Bethesda (MD): National Library of Medicine (US), National Center for Biotechnology Information; 2004 [Available from: <https://pubchem.ncbi.nlm.nih.gov/compound/Pyridine>].
88. Mohammad Abu-Taweel G, Ibrahim MM, Khan S, Al-Saidi HM, Alshamrani M, Alhumaydhi FA, et al. Medicinal Importance and Chemosensing Applications of Pyridine Derivatives: A Review. *Crit Rev Anal Chem.* 2022:1-18.
89. Scriven EFV, Toomey Jr. JE, Murugan R. Pyridine and Pyridine Derivatives. *Kirk-Othmer Encyclopedia of Chemical Technology.*
90. Pandey RA, Padoley KV, Mukherji SS, Mudliar SN, Vaidya AN, Rajvaidya AS, et al. Biotreatment of waste gas containing pyridine in a biofilter. *Bioresour Technol.* 2007;98(12):2258-67.
91. Huang C, Chen S, Lai C, Reneker DH, Qiu H, Ye Y, et al. Electrospun polymer nanofibres with small diameters. *Nanotechnology.* 2006;17(6):1558-63.
92. Koniarczyk JL, Hesk D, Overgard A, Davies IW, McNally A. A General Strategy for Site-Selective Incorporation of Deuterium and Tritium into Pyridines, Diazines, and Pharmaceuticals. *J Am Chem Soc.* 2018;140(6):1990-3.

93. Guan AY, Liu CL, Sun XF, Xie Y, Wang MA. Discovery of pyridine-based agrochemicals by using Intermediate Derivatization Methods. *Bioorg Med Chem.* 2016;24(3):342-53.
94. Vaganova E, Eliaz D, Shimanovich U, Leitus G, Aqad E, Lokshin V, et al. Light-Induced Reactions within Poly(4-vinyl pyridine)/Pyridine Gels: The 1,6-Polyazaacetylene Oligomers Formation. *Molecules.* 2021;26(22).
95. Levy JN, Alegre-Requena JV, Liu R, Paton RS, McNally A. Selective Halogenation of Pyridines Using Designed Phosphine Reagents. *J Am Chem Soc.* 2020;142(25):11295-305.
96. Alizadeh SR, Ebrahimzadeh MA. Antiviral Activities of Pyridine Fused and Pyridine Containing Heterocycles, A Review (from 2000 to 2020). *Mini Rev Med Chem.* 2021;21(17):2584-611.
97. Ling Y, Hao ZY, Liang D, Zhang CL, Liu YF, Wang Y. The Expanding Role of Pyridine and Dihydropyridine Scaffolds in Drug Design. *Drug Des Devel Ther.* 2021;15:4289-338.
98. Zuo Y. Treatment of the Rust Layer by Different Pyridine Derivatives and Its Effect on the Epoxy-Polyvinylbutyral Coating Directly Painted onto the Rust Mild Steel. *International Journal of Electrochemical Science.* 2017;12:11728-41.
99. Tang Z, Wu X, Guo B, Zhang L, Jia D. Preparation of butadiene–styrene–vinyl pyridine rubber–graphene oxide hybrids through co-coagulation process and in situ interface tailoring. *J Mater Chem.* 2012;22:7492-501.
100. Tsygankova V, Ya.V A, O.I S, R.M S, Hurenko A, Frasinuk M, et al. Study of auxin-like and cytokinin-like activities of derivatives of pyrimidine, pyrazole, isoflavones, pyridine, oxazolopyrimidine and oxazole on haricot bean and pumpkin plants. *Int J Chem Tech* 2018;11:174-90.
101. Quiryneen M, Soers C, Desnyder M, Dekeyser C, Pauwels M, van Steenberghe D. A 0.05% cetyl pyridinium chloride/0.05% chlorhexidine mouth rinse during maintenance phase after initial periodontal therapy. *J Clin Periodontol.* 2005;32(4):390-400.
102. Imazato S, Russell RR, McCabe JF. Antibacterial activity of MDPB polymer incorporated in dental resin. *J Dent.* 1995;23(3):177-81.
103. de Faria NS, Moura LKB, de Macedo LMD, Colucci V, Raucchi-Neto W, Messias DC.

Effect of a 12-methacryloyloxy-dodecyl-pyridinium-bromide-containing adhesive with different post types on the long-term bond strength to dentin. *Eur J Oral Sci.* 2017;125(5):403-9.

104. Perdigão J, Reis A, Loguercio AD. Dentin adhesion and MMPs: a comprehensive review. *J Esthet Restor Dent.* 2013;25(4):219-41.

105. Frisby CL, Mattsson JP, Jensen JM, Lehmann A, Dent J, Blackshaw LA. Inhibition of transient lower esophageal sphincter relaxation and gastroesophageal reflux by metabotropic glutamate receptor ligands. *Gastroenterology.* 2005;129(3):995-1004.

106. Stone EA, Cutrona KJ, Miller SJ. Asymmetric Catalysis upon Helically Chiral Loratadine Analogues Unveils Enantiomer-Dependent Antihistamine Activity. *J Am Chem Soc.* 2020;142(29):12690-8.

107. Iqbal J, Gupta A, Husain A. Photochemistry of phenazopyridine hydrochloride. *Pharmazie.* 2006;61(9):747-50.

108. Onder AM, Espinoza V, Berho ME, Chandar J, Zilleruelo G, Abitbol C. Acute renal failure due to phenazopyridine (Pyridium) overdose: case report and review of the literature. *Pediatr Nephrol.* 2006;21(11):1760-4.

109. Bekatorou A. Alcohol: Properties and determination. Oxford: Academic Press; 2016. 88-96 p.

110. Huang Z, Wu P, Yin Y, Zhou X, Fu L, Wang L, et al. Preparation of pyridine-modified cotton fibers for anionic dye treatment. *Reactive and Functional Polymers.* 2022;172:105155.

111. Lara J, Zimmermann F, Drolet D, Hansen C, Chollot A, Monta N. The use of the Hansen solubility parameters in the selection of protective polymeric materials resistant to chemicals. *International Journal of Current Research.* 2017;9:47860-7.

112. Kneisl P, Zondlo JW. Vapor pressure, liquid density, and the latent heat of vaporization as functions of temperature for four dipolar aprotic solvents. *Journal of Chemical & Engineering Data.* 1987;32(1):11-3.

113. Han K, Jeon G, Hong I, Lee SB. Prediction of solubility parameter from intrinsic viscosity. *Journal of Industrial and Engineering Chemistry.* 2013;19:1130-6.

114. Hansen CM. The Universality of the Solubility Parameter. *Product R&D.* 1969;8(1):2-11.

115. Miller-Chou BA, Koenig JL. A review of polymer dissolution. *Progress in Polymer Science*. 2003;28(8):1223-70.
116. Barton AFM. Solubility parameters. *Chemical Reviews*. 1975;75(6):731-53.
117. Pitera JW, van Gunsteren WF. The importance of solute-solvent van der Waals interactions with interior atoms of biopolymers. *J Am Chem Soc*. 2001;123(13):3163-4.
118. Hermann J, DiStasio RA, Jr., Tkatchenko A. First-Principles Models for van der Waals Interactions in Molecules and Materials: Concepts, Theory, and Applications. *Chem Rev*. 2017;117(6):4714-58.
119. Hansen CM, editor *The three dimensional solubility parameter - key to paint component affinities: I. Solvents, plasticizers, polymers, and resins* 1967.
120. Hansen CM, editor *The three-dimensional solubility parameter - key to paint component affinities: solvents, plasticizers, polymers, and resins. II. Dyes, emulsifiers, mutual solubility and compatibility, and pigments. III. Independent calculation of the parameter components* 1967.
121. Bristow GM, Watson WF. Cohesive energy densities of polymers. Part 1.— Cohesive energy densities of rubbers by swelling measurements. *Transactions of the Faraday Society*. 1958;54(0):1731-41.
122. Hildebrand JH. *Factors Determining Solubility among Non-Electrolytes*. *Proc Natl Acad Sci U S A*. 1950;36(1):7-15.
123. Barton AFM. Applications of solubility parameters and other cohesion parameters in polymer science and technology. *Pure and Applied Chemistry*. 1985;57:905 - 12.
124. Adamska K, Voelkel A, Héberger K. Selection of solubility parameters for characterization of pharmaceutical excipients. *J Chromatogr A*. 2007;1171(1-2):90-7.
125. Breitzkreutz J. Prediction of intestinal drug absorption properties by three-dimensional solubility parameters. *Pharm Res*. 1998;15(9):1370-5.
126. Srinivas K, King JW, Monrad JK, Howard LR, Hansen CM. Optimization of subcritical fluid extraction of bioactive compounds using Hansen solubility parameters. *J Food Sci*. 2009;74(6):E342-54.
127. Guo X, Spencer P, Wang Y, Ye Q, Yao X, Williams K. Effects of a solubility enhancer on penetration of hydrophobic component in model adhesives into wet

demineralized dentin. *Dent Mater.* 2007;23(12):1473-81.

128. Castellan CS, Pereira PN, Viana G, Chen SN, Pauli GF, Bedran-Russo AK. Solubility study of phytochemical cross-linking agents on dentin stiffness. *J Dent.* 2010;38(5):431-6.

129. Belmares M, Blanco M, Goddard WA, 3rd, Ross RB, Caldwell G, Chou SH, et al. Hildebrand and Hansen solubility parameters from molecular dynamics with applications to electronic nose polymer sensors. *J Comput Chem.* 2004;25(15):1814-26.

130. Inglev R, Woyessa G, Bang O, Janting J. Polymer Optical Fiber Modification By Etching Using Hansen Solubility Parameters—A Case Study of TOPAS, Zeonex, and PMMA. *Journal of Lightwave Technology.* 2019;37(18):4776-83.

131. Medina-Castillo AL, Fernandez-Sanchez JF, Segura-Carretero A, Fernandez-Gutierrez A. A semi-empirical model to simplify the synthesis of homogeneous and transparent cross-linked polymers and their application in the preparation of optical sensing films. *Biosens Bioelectron.* 2009;25(2):442-9.

132. Nielsen T, Hansen C. Elastomer swelling and Hansen solubility parameters. *Polymer Testing - POLYM TEST.* 2005;24:1054-61.

133. Hansen C, Just L. Prediction of Environmental Stress Cracking in Plastics with Hansen Solubility Parameters. *Industrial & Engineering Chemistry Research - IND ENG CHEM RES.* 2000;40.

134. Vallittu PK, Ruyter IE, Nat R. The swelling phenomenon of acrylic resin polymer teeth at the interface with denture base polymers. *J Prosthet Dent.* 1997;78(2):194-9.

135. Li H, Xiao R. Glass Transition Behavior of Wet Polymers. *Materials (Basel).* 2021;14(4).

136. Karlsson O, Stubbs J, Karlsson L, Sundberg D. Estimating diffusion coefficients for small molecules in polymers and polymer solutions. *Polymer.* 2001;42:4915-23.

137. Gugliuzza A, Drioli E. PVDF and HYFLON AD membranes: Ideal interfaces for contactor applications. *Journal of Membrane Science.* 2007;300(1):51-62.

138. Buckley DJ, Berger M. The swelling of polymer systems in solvents. II. Mathematics of diffusion. *Journal of Polymer Science.* 1962;56(163):175-88.

139. Fedors RF. A method for estimating both the solubility parameters and molar volumes of liquids. *Polymer Engineering & Science.* 1974;14(2):147-54.

140. Gupta N, Srivastava AK. Interpenetrating polymer networks: A review on synthesis and properties. *Polymer International*. 1994;35(2):109-18.
141. Sperling LH. Interpenetrating Polymer Networks. In: Klemptner D SL, Utracki LA, editor. *Interpenetrating Polymer Networks*. NY: American Chemical Society; 1994. p. 3-38.
142. Sperling LH. Interpenetrating polymer networks and related materials. *Journal of Polymer Science: Macromolecular Reviews*. 1977;12(1):141-80.
143. Leach R. Introduction to Surface Texture Measurement. In: Leach R, editor. *Optical Measurement of Surface Topography*. Berlin, Heidelberg: Springer Berlin Heidelberg; 2011. p. 1-14.
144. Whitehead SA, Shearer AC, Watts DC, Wilson NH. Comparison of methods for measuring surface roughness of ceramic. *J Oral Rehabil*. 1995;22(6):421-7.
145. McCool JI. Assessing the Effect of Stylus Tip Radius and Flight on Surface Topography Measurements. *Journal of Tribology-transactions of The Asme*. 1984;106:202-9.
146. International Organization for Standardization. *Geometrical Product Specifications (GPS)–Surface Texture: Profile Method; Measurement Standards–Part 1: Material Measures*. Geneva: International Organization for Standardization; 2000.
147. Ki-Hwan K, Nahm-Gyoo C. Assessing the effect of stylus tip radius on surface roughness measurement by accumulation spectral analysis. *International Journal of Precision Engineering and Manufacturing*. 2006;7(1):9-12.
148. Radhakrishnan VM. Effect of stylus radius on the roughness values measured with tracing stylus instruments. *Wear*. 1970;16:325-35.
149. O'Donnell KA. Effects of finite stylus width in surface contact profilometry. *Appl Opt*. 1993;32(25):4922-8.
150. Lee D-H, Cho NG. Assessment of surface profile data acquired by a stylus profilometer. *Measurement Science & Technology - MEAS SCI TECHNOL*. 2012;23.
151. Field J, Waterhouse P, German M. Quantifying and qualifying surface changes on dental hard tissues in vitro. *J Dent*. 2010;38(3):182-90.
152. Sturm S, Jančar B. Chapter 8 - Microstructure Characterization of Advanced Ceramics. In: Shen JZ, Kosmač T, editors. *Advanced Ceramics for Dentistry*. Oxford:

Butterworth-Heinemann; 2014. p. 151-72.

153. Marshall GW, Jr., Marshall SJ, Balooch M, Kinney JH. Evaluating demineralization and mechanical properties of human dentin with AFM. *Methods Mol Biol.* 2004;242:141-59.
154. Chen F, Brown G, Song M. Overview of 3-D shape measurement using optical methods. *Optical Engineering.* 2000;39(1):10-22.
155. Watson TF. Applications of confocal scanning optical microscopy to dentistry. *Br Dent J.* 1991;171(9):287-91.
156. Elliott AD. Confocal Microscopy: Principles and Modern Practices. *Curr Protoc Cytom.* 2020;92(1):e68.
157. Hovis DB, Heuer AH. The use of laser scanning confocal microscopy (LSCM) in materials science. *J Microsc.* 2010;240(3):173-80.
158. Ihrke I, Kutulakos K, Lensch H, Magnor M, Heidrich W. Transparent and Specular Object Reconstruction. *Comput Graph Forum.* 2010;29:2400-26.
159. Conroy M, Armstrong J. A comparison of surface metrology techniques. *Journal of Physics: Conference Series.* 2006;13:458.
160. Caber PJ. Interferometric profiler for rough surfaces. *Appl Opt.* 1993;32(19):3438-41.
161. Pavliček P, Mikeska E. White-light interferometer without mechanical scanning. *Optics and Lasers in Engineering.* 2020;124:105800.
162. Yang S, Guofeng Z. A review on interferometry for geometric measurement. *Measurement Science and Technology.* 2018;29.
163. Baryshev SV, Erck RA, Moore JF, Zinovev AV, Tripa CE, Veryovkin IV. Characterization of surface modifications by white light interferometry: applications in ion sputtering, laser ablation, and tribology experiments. *J Vis Exp.* 2013(72):e50260.
164. Stenhagen KR, Hove LH, Holme B, Tveit AB. Enamel erosion depths measured on impressions by a white light interferometer. *Acta Odontol Scand.* 2013;71(3-4):398-403.
165. Holme B, Hove LH, Tveit AB. Using white light interferometry to measure etching of dental enamel. *Measurement.* 2005;38(2):137-47.
166. Park JB, Yang SM, Ko Y. Evaluation of the Surface Characteristics of Various

Implant Abutment Materials Using Confocal Microscopy and White Light Interferometry. *Implant Dent.* 2015;24(6):650-6.

167. Kournetas N, Spintzyk S, Schweizer E, Sawada T, Said F, Schmid P, et al. Comparative evaluation of topographical data of dental implant surfaces applying optical interferometry and scanning electron microscopy. *Dent Mater.* 2017;33(8):e317-e27.

168. Faul F, Erdfelder E, Lang AG, Buchner A. G*Power 3: a flexible statistical power analysis program for the social, behavioral, and biomedical sciences. *Behav Res Methods.* 2007;39(2):175-91.

169. Sorensen JA, Engelman MJ. Ferrule design and fracture resistance of endodontically treated teeth. *J Prosthet Dent.* 1990;63(5):529-36.

170. Hochman N, Feinzaig I, Zalkind M. Effect of design of pre-fabricated posts and post heads on the retention of various cements and core materials. *J Oral Rehabil.* 2003;30(7):702-7.

171. Rasimick BJ, Wan J, Musikant BL, Deutsch AS. A review of failure modes in teeth restored with adhesively luted endodontic dowels. *J Prosthodont.* 2010;19(8):639-46.

172. Signore A, Benedicenti S, Kaitsas V, Barone M, Angiero F, Ravera G. Long-term survival of endodontically treated, maxillary anterior teeth restored with either tapered or parallel-sided glass-fiber posts and full-ceramic crown coverage. *J Dent.* 2009;37(2):115-21.

173. Monticelli F, Goracci C, Grandini S, Garcia-Godoy F, Ferrari M. Scanning electron microscopic evaluation of fiber post-resin core units built up with different resin composites. *Am J Dent.* 2005;18(1):61-5.

174. Monticelli F, Goracci C, Ferrari M. Micromorphology of the fiber post-resin core unit: a scanning electron microscopy evaluation. *Dent Mater.* 2004;20(2):176-83.

175. Sano H, Shono T, Sonoda H, Takatsu T, Ciucchi B, Carvalho R, et al. Relationship between surface area for adhesion and tensile bond strength--evaluation of a micro-tensile bond test. *Dent Mater.* 1994;10(4):236-40.

176. Pashley DH, Sano H, Ciucchi B, Yoshiyama M, Carvalho RM. Adhesion testing of dentin bonding agents: a review. *Dent Mater.* 1995;11(2):117-25.

177. Della Bona A, van Noort R. Shear vs. tensile bond strength of resin composite

- bonded to ceramic. *J Dent Res.* 1995;74(9):1591-6.
178. Poitevin A, De Munck J, Van Landuyt K, Coutinho E, Peumans M, Lambrechts P, et al. Critical analysis of the influence of different parameters on the microtensile bond strength of adhesives to dentin. *J Adhes Dent.* 2008;10(1):7-16.
179. Goracci C, Sadek FT, Monticelli F, Cardoso PE, Ferrari M. Influence of substrate, shape, and thickness on microtensile specimens' structural integrity and their measured bond strengths. *Dent Mater.* 2004;20(7):643-54.
180. Sadek FT, Cury AH, Monticelli F, Ferrari M, Cardoso PE. The influence of the cutting speed on bond strength and integrity of microtensile specimens. *Dent Mater.* 2005;21(12):1144-9.
181. Eckert GJ, Platt JA. A statistical evaluation of microtensile bond strength methodology for dental adhesives. *Dent Mater.* 2007;23(3):385-91.
182. Mallmann A, Jacques LB, Valandro LF, Muench A. Microtensile bond strength of photoactivated and autopolymerized adhesive systems to root dentin using translucent and opaque fiber-reinforced composite posts. *J Prosthet Dent.* 2007;97(3):165-72.
183. Machry RV, Fontana PE, Bohrer TC, Valandro LF, Kaizer OB. Effect of Different Surface Treatments of Resin Relined Fiber Posts Cemented With Self-adhesive Resin Cement on Push-out and Microtensile Bond Strength Tests. *Oper Dent.* 2020;45(4):E185-e95.
184. Navarro CA, Kedzie EA, Ma Y, Michael KH, Nutt SR, Williams TJ. Mechanism and Catalysis of Oxidative Degradation of Fiber-Reinforced Epoxy Composites. *Top Catal.* 2018;61(7-8):704-9.
185. Menezes MS, Faria-e-Silva AL, Silva FP, Reis GR, Soares CJ, Stape TH, et al. Etching a fiber post surface with high-concentration bleaching agents. *Oper Dent.* 2014;39(1):E16-21.
186. Majeti C, Veeramachaneni C, Morisetty PK, Rao SA, Tummala M. A simplified etching technique to improve the adhesion of fiber post. *J Adv Prosthodont.* 2014;6(4):295-301.
187. Miller RG, Bowles CQ, Chappelow CC, Eick JD. Application of solubility parameter theory to dentin-bonding systems and adhesive strength correlations. *J Biomed Mater Res.* 1998;41(2):237-43.

188. Pashley DH, Tay FR, Carvalho RM, Rueggeberg FA, Agee KA, Carrilho M, et al. From dry bonding to water-wet bonding to ethanol-wet bonding. A review of the interactions between dentin matrix and solvated resins using a macromodel of the hybrid layer. *Am J Dent.* 2007;20(1):7-20.
189. Kiomarsi N, Saburian P, Chiniforush N, Karazifard MJ, Hashemikamangar SS. Effect of thermocycling and surface treatment on repair bond strength of composite. *J Clin Exp Dent.* 2017;9(8):e945-e51.
190. Özcan M, Corazza PH, Marocho SM, Barbosa SH, Bottino MA. Repair bond strength of microhybrid, nanohybrid and nanofilled resin composites: effect of substrate resin type, surface conditioning and ageing. *Clin Oral Investig.* 2013;17(7):1751-8.
191. Gale MS, Darvell BW. Thermal cycling procedures for laboratory testing of dental restorations. *J Dent.* 1999;27(2):89-99.
192. Ghavami-Lahiji M, Firouzmanesh M, Bagheri H, Jafarzadeh Kashi TS, Razazpour F, Behroozibakhsh M. The effect of thermocycling on the degree of conversion and mechanical properties of a microhybrid dental resin composite. *Restor Dent Endod.* 2018;43(2):e26.
193. Stewardson DA, Shortall AC, Marquis PM. The effect of clinically relevant thermocycling on the flexural properties of endodontic post materials. *J Dent.* 2010;38(5):437-42.
194. Lassila LV, Tanner J, Le Bell AM, Narva K, Vallittu PK. Flexural properties of fiber reinforced root canal posts. *Dent Mater.* 2004;20(1):29-36.



จุฬาลงกรณ์มหาวิทยาลัย
CHULALONGKORN UNIVERSITY

VITA

NAME Wisarut Prawatvatchara

DATE OF BIRTH 1 พฤศจิกายน 2531

PLACE OF BIRTH กรุงเทพมหานคร

INSTITUTIONS ATTENDED 2014 Doctor of Dental Surgery (D.D.S.)
Mahidol University, Thailand
2018 Higher Graduate Diploma of Clinical Sciences
Program in Prosthodontics Department of Prosthodontic,
Faculty of Dentistry, Chulalongkorn University, Bangkok,
Thailand
2020 Diplomate, Thai Board of Prosthodontics
2019-2023 Student of PhD in Prosthodontics ,
Department of Prosthodontic, Faculty of Dentistry,
Chulalongkorn University, Bangkok, Thailand

HOME ADDRESS 53/3 ประดิพัทธ์ 15 สามเสนใน พญาไท กทม 10400

PUBLICATION - Prawatvatchara W, Surintanasarn A,
Thamrongananskul N. Simplified technique of palatal
augmentation prosthesis to increase swallow efficiency in
a partial glossectomy patient: a case report Thammasat
Medical Journal Vol. 20 No. 1 (2020): January-March.
- Prawatvatchara W, Sriamporn T, Klaisiri A,
Thamrongananskul N. Radiopacity of 9 Clear Resin
Cements and Zinc Phosphate Cement. KDJ [Internet].
2021 Mar. 3
- Prawatvatchara W, Limpuangthip N,
Techapiroonthong S, Thamrongananskul N. Three-piece
digital complete denture obturator with a heptagonal key
assembly for a patient with a total maxillectomy: A dental

technique. J Prosthet Dent. 2023 Jul 10:S0022-3913(23)00413-4.



จุฬาลงกรณ์มหาวิทยาลัย
CHULALONGKORN UNIVERSITY